Graphical Abstract

Degradation modelling of external grouted post-tensioning tendons: numerical assessment under corrosion conditions

Belén Vecino, Carlos M. C. Renedo, Jaime H. García-Palacios, Iván M. Díaz

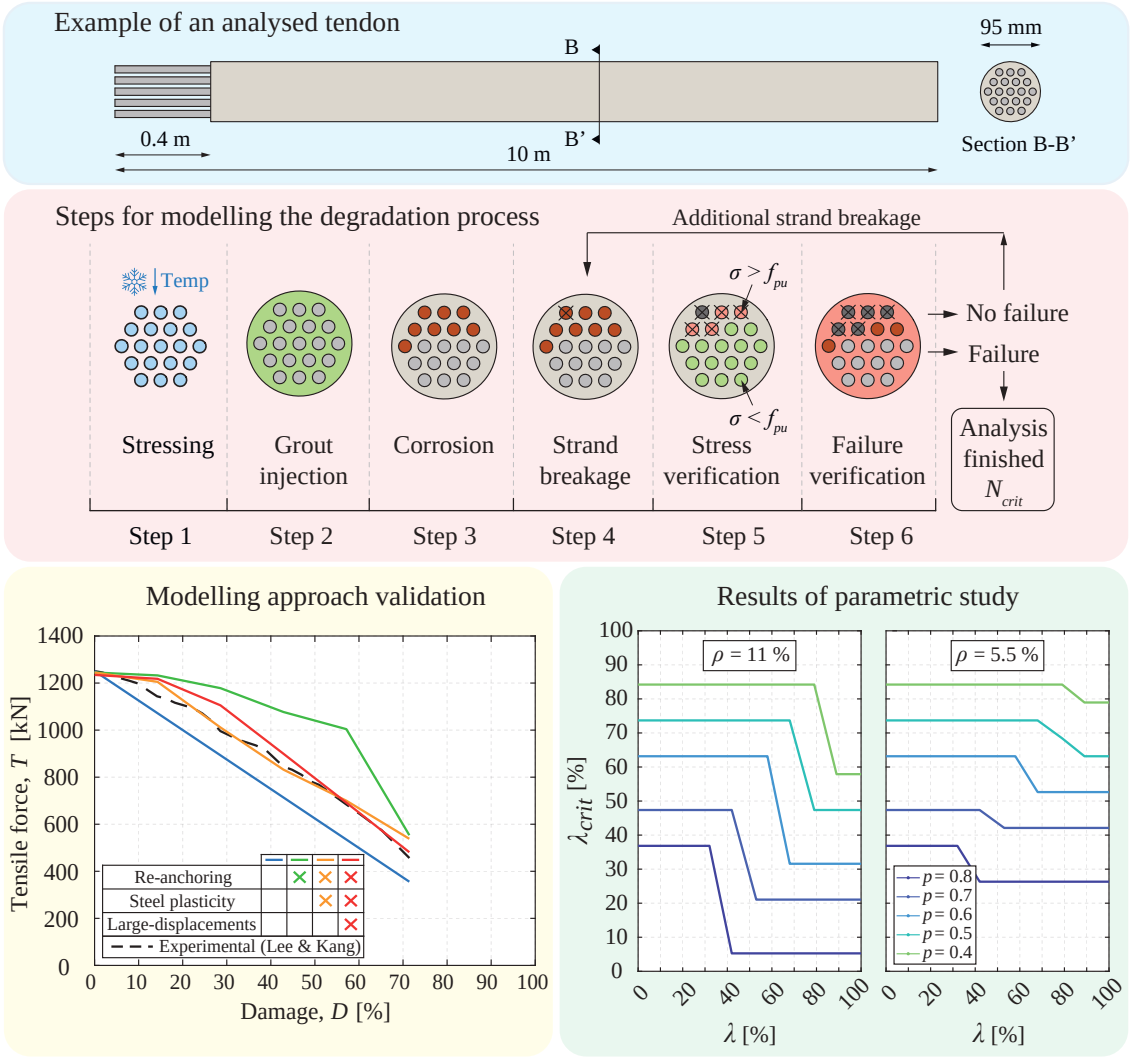

Highlights

Degradation modelling of external grouted post-tensioning tendons: numerical assessment under corrosion conditions

Belén Vecino, Carlos M. C. Renedo, Jaime H. García-Palacios, Iván M. Díaz

- Research highlight 1

  A non-linear modelling approach of the degradation process of external grouted post-tensioning tendons due to corrosion is presented. The approach considers the influence of steel plasticity, large deformations and grout-strand contact stiffness together with a corrosion degree in some strands.

- Research highlight 2

  The degradation curves (tendon tensile force versus grade of damage, natural frequencies versus grade of damage) are useful for setting the sensitivity and thresholds of performance indicators in the case of continuous dynamic monitoring systems.

- Research highlight 3

  The proposed modelling approach allows to carry out parametric studies to assess which corrosion conditions are critical and may lead to tendon failure. The parameters studied are: i) the initial stressing force, ii) the corrosion degree of the section and, iii) the proportion of the steel area of the section affected by corrosion.

- Research highlight 4

The parametric study is geared to engineering practice, as it is a convenient tool that can be used in bridge inspections to determine the risk of a tendon failure.

Degradation modelling of external grouted post-tensioning tendons: numerical assessment under corrosion conditions

Belén Vecino[a], Carlos M. C. Renedo[a], Jaime H. García-Palacios[b], Iván M. Díaz[a]

[a]*Department of Continuum Mechanics and Theory of Structures, ETSI Caminos, Canales y Puertos, Universidad Politécnica de Madrid, Calle Profesor Aranguren 3, Madrid, 28040, Comunidad de Madrid, Spain*
[b]*Department of Hydraulics, Energy and Environmental Engineering, ETSI Caminos, Canales y Puertos, Universidad Politécnica de Madrid, Calle Profesor Aranguren 3, Madrid, 28040, Comunidad de Madrid, Spain*

Abstract

In the last years, several brittle fractures of external bonded post-tensioning tendons in bridges have been reported due to corrosion damage, compromising the structural safety and stability of the bridges. This paper proposes a finite element non-linear modelling approach of grouted tendons to study their mechanical behaviour and risk of failure when a level and extent of corrosion of the steel strands is assumed. This approach has been first validated with the experimental tests previously presented in the literature, thus analysing the influence of the steel plasticity, large deformations and re-anchoring effect, in order to reproduce accurately the experimental tests, qualitative and quantitative. The degradation curves are derived, that is, the effective tensile force and natural frequencies versus the percentage of damage, which is defined as the percentage of broken strands, and are compared with experimental tests. Then, a parametric study is performed using the

proposed modelling strategy. The objective is evaluate the critical number of strands broken for tendon failure depending on its corrosion condition, which is defined by two parameters: i) the number of corroded strands within the tendon, and ii) the corrosion degree of the strands. The initial stressing force of the tendon has been included within the parametric study, this is determinant in the stress redistribution and in a possible tendon failure when a strand breaks.
Keywords: Post-tensioning tendons, Grouted external tendons, Bonded tendons, Corrosion induced failure, Non-linear FE modelling

1. Introduction

External post-tensioning is a construction technology commonly used in highway and railway concrete box-girder bridges. It is usually applied by means of external post-tensioning tendons placed inside the box girder of the bridge deck, but outside the concrete cross-section, as seen in Figure 1. The stressing force is transferred to the concrete girder through anchorages and deviators [1]. The main advantages of this technology, which have led to its popularisation, are: i) it allows the substitution of the tendons if there are wires or strands broken, which may occur due to corrosion, as illustrated in Figure 2, and ii) the ability to perform their re-tensioning if their tensile force is significantly lower than the stressing force. These actions contribute to increase the durability of these structures at a limited cost [2], [3]. In addition, external post-tensioning has other advantages, such as economical and rapid construction and easy inspections, monitoring, and maintenance.

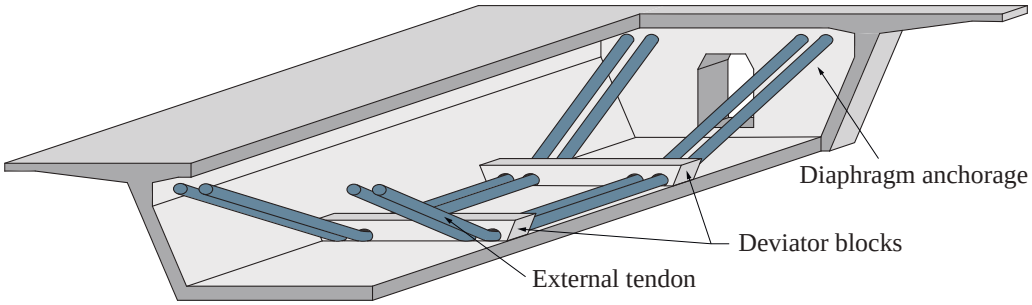

Figure 1: Box girder with external prestressing.

Figure 2: Broken tendon affected by corrosion [1].

External tendons consist of prestressing steel strands, typically seven-wire strands, surrounded by a corrosion protection material. There are two main types: bonded and unbonded[1]. In bonded tendons, also known as grouted tendons, corrosion protection is provided by a metal or polyethylene sheath-

[1]Bonded and unbonded terminology is frequently used in the field of prestressed concrete to describe the compatibility between an internal prestressed tendon and the surrounding concrete mass.

ing duct filled with grout, which adheres to the strands [2, 4], as depicted in Figure 3 (a). Unbonded tendons have a sheathing duct around the strands, sometimes filled with grout, but each strand is encased in a monostrand duct filled with non-adherent material such as grease or wax [2], Figure 3 (b). Unlike bonded tendons, unbonded strands can slip and, in case of breakage, they return to their unloaded length. This paper focuses on bonded tendons, which were widely used until the first decade of this century, and most reported corrosion cases involve this type.

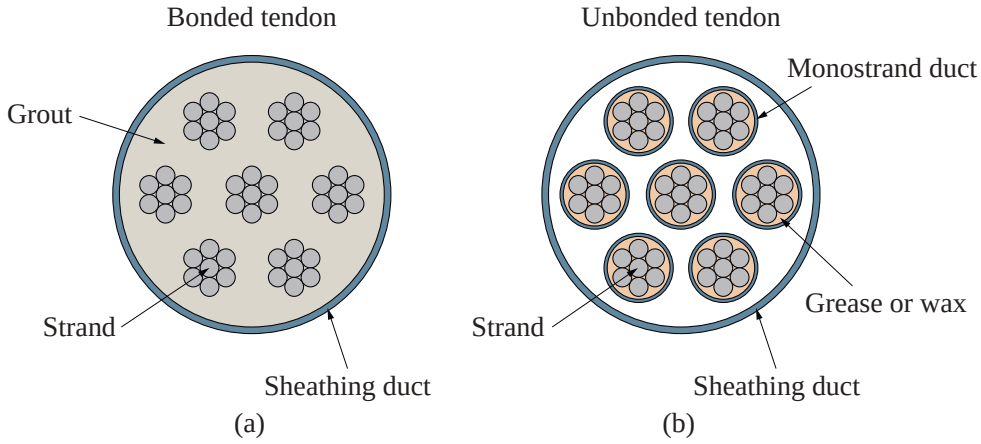

Figure 3: (a) Bonded tendon cross-section. (b) Unbonded tendon cross-section

1.1. History summary of external post-tensioning systems

External bonded post-tensioning tendons have been used since the beginning of the 1950s, when four box-girder bridges were constructed in France, although this system was not widely used until the 1980s [3]. These first four bridges are: the Vaux sur Seine Bridge, the Port à Binson Bridge, The Villeneuve Saint-Georges Bridge and the Can Bia Bridge [3]. The extended use

of this technology was popularized during the 1970s, especially in France and the United States, pioneer countries in the use of external post-tensioning tendons. At that time, external post-tensioning was mainly used for reinforcement and rehabilitation of existing bridges [3], [5]. Since the 1980s, the use of external post-tensioning tendons has been extended in new construction due to their technical and constructive advantages, especially due to the ease of inspection and maintenance [1]. Since that decade, external post-tensioning has been mainly used in constructing continuous bridges, precast segmental bridges, balanced-cantilever bridges, and extradosed and cable-stayed bridges. In some cases, external post-tensioning systems are key elements for structural stability, as in precast segmental bridges; in others, they contribute to the stiffening of the structure as in launched or balanced-cantilever bridges.

1.2. Issues of external grouted post-tensioning tendons

The main issue related to external grouted post-tensioning tendons is that when strand breakage occurs, the grout prevents the broken strand from sliding inside the grout due to friction. This implies that the broken strand is re-anchored into the grout, transferring its tensile force to the rest of the adjacent healthy strands, which locally increase their tensile stress in the surroundings of the breakage [6], [7]. The damage region is related to a transfer length, which is the distance required for the strands to hold almost their original tensile stress [8]. Thus, there is no significant decrease in the total tensile force of the tendon caused by the breakage of some of its strands. In some cases, if many strands of the tendon are corroded, this increase in tensile stress may exceed the tendon's capacity to assume additional stresses,

provoking its brittle failure, as seen in Figure 2. In unbonded tendons, this mechanical behaviour does not occur because when one strand breaks, it slides into its mono-strand duct and gets completely de-tensioned, producing the loss of its contributing tensile force and not transferring it to the rest of the strands.

Proper grout injection is one of the main concerns related to the construction of external grouted tendons. To ensure that, since the 1980s, the use of superplasticisers and grout additives became popular. However, in many cases, the adequate filling of the duct was not actually achieved; furthermore, the use of some of these additives facilitated the segregation of minerals formed during the set of the grout. As a result of this, a wet, white paste that hardened with air and a yellowish liquid with strong alkalinity appeared inside the duct, especially near anchorages located at a certain height, where segregation is facilitated [9], [10]. Hence, the presence of air in combination with an alkaline liquid led to the corrosion of the affected tendons, which occasionally resulted in their brittle collapse.

These brittle failures have been reported since the late 1990s mainly in France and the United States [11]. This situation triggered the creation of technical reports by the Florida Department of Transportation (FDOT) in the United States, and Sétra in France, where information, recommendations and safety instructions regarding the corrosion and failure of external grouted tendons built between the years 1980 and 2000 were presented. For example, based on this, in France, the use of external grouted tendons was prohibited. Since then, additional tendon failures have been reported due to stress corrosion cracking situations, caused by the interaction of corrosion

and mechanical stress. These failures have been produced by several causes such as i) deficient grout injection procedures leading to voids in the duct and anchorages [1], [2], [11], ii) presence of additives and water in the mortar [3], iii) unsuitable grouting materials [2], [4], iv) segregation processes of the solid content of the mortar, which leaves the water in contact with the steel in the presence of corrosive agents [11], v) cracked polyethylene duct [2], among others. Some significant bridges affected by these problems are gathered in Table 1, in which examples of externally prestressed concrete bridges and cable-stayed bridges are included, since in both cases grout is used as corrosion protection and then they experience similar corrosion problems.

Table 1: Examples of externally prestressing bridges and cable-stayed bridges that have experienced corrosion problems [1], [2], [10].

Bridge	Year*	Country	Span [m]	Length [m]
Morandi bridge	1967 (2018)	Italy	210	1182
Saint-Cloud viaduct	1974 (1998)	France	102	1000
Sunshine Skyway bridge	1982 (1988)	EEUU	366	6663
Niles Channel Bridge	1983 (1999)	EEUU	36	1389
Bridge over the Durance	1986 (1994)	France	51	288
Puente Fernando Reig	1987 (2016)	Spain	132	246
Ile de Ré bridge	1988 (2018)	France	110	2962
Varina-Enon bridge	1990 (2007)	EEUU	190	1430
Riviere d'Abord bridge	1991 (2001)	France	50	150
Mid-Bay bridge	1993 (2000)	EEUU	69	5794
Lowe's Motor Speedway bridge	1995 (2000)	EEUU	24	96
Viaducto de O Castro	1997 (2022)	Spain	50	585
Viaducto de Río Blanco	1998 (2021)	Spain	48	558
Viaducto de Guiniguada	2003 (2024)	Spain	140	288

*Construction Year (Year in which the corrosion problem was discovered)

1.3. Degradation of external grouted tendons: experimental works

There are not many experimental research works on the mechanical behaviour of external post-tensioning tendons, bonded or unbonded, against progressive degradation due to corrosion in which the tensile force loss is quantified. As for unbonded tendons, Abdullah et al. [12] have studied the progressive rupture of wires in confined and unconfined conditions. Also, they have tested an unbonded tendon of six seven-wire strands filled with wax in

which successive wire cuts were performed up to break the seven wires, that is, the complete strand. A significant decrease in the tensile force was observed for every wire cut in a location away from the breakage for unconfined and confined strands. Regarding grouted tendons, Wood et al. [7] have studied the influence of increasing corrosion damage on bonded post-tensioning tendons by means of laboratory tests. It is observed that the decrease of the tensile force is slower than the loss of the steel cross-sectional area of the strands. In addition, a stress redistribution from the broken strands to the adjacent strands is noticeable, making apparent the re-anchoring phenomenon and its inherent non-linear nature. This evidences that assuming a linear decrease of the tensile force due to damage is not appropriate. Later, and based on similar tests of those carried out by Wood et al. [7], Lee and Kang [13] have studied the change in the dynamic properties of these grouted tendons when damage progresses. There, the variation of the natural frequencies and the tensile force of the tendons is investigated when corrosion is induced into a tendon section. It is determined that the tensile force is the main structural parameter affected by the damage level in the tendon and that the variation of the frequency response function is more subtle, although higher frequencies are more sensitive to damage than lower frequencies. Similarly, Kim et al. [14] have studied three grouted tendons of three strands each, subjected to progressive corrosion. Again, stress redistribution due to the strands' re-anchoring is detected. One of the most complete contributions regarding the mechanical behaviour of grouted post-tensioning tendons under corrosion is the one recently developed by Aparicio et al. [8]. The authors have carried out experimental tests on different tendons to determine

the influence of the number of strands, the brittleness of the duct, and the cutting schedule on the re-anchoring phenomenon. Also, a model has been developed to estimate the transfer length associated with this re-anchoring based on the measurement of the sliding of the wire after its breakage.

Other experimental researches developed by Losanno et al. [15], [16] address the impact of three factors: i) the presstressing level, ii) partial grouting, and iii) the presence of corroded strands on the load bearing capacity of internally post-tensioned concrete girders. Their main conclusion is that the strands' corrosion is the main parameter that diminishes the capacity of this type of beams, and that the damage location impacts the girders' performance. It is also underscored the critical role of grouting conditions and prestressing levels in flexural performance.

1.4. Degradation of external grouted tendons: FE modelling

Regarding FE modelling, several studies on the behaviour of single strands (Ghoreishi et al. [17], Foti and de Luca di Roseto [18], de Menezes et al. [19], Abdullah et al. [20]) can be found in the literature. The influence of the interaction between the wires into the strand is addressed, and this friction effect is noted to have little influence on the global response of the strand [17], [18]. However, FE modelling approaches of a complete grouted tendon are limited. As for bonded internal tendons, Brenkus et al. [21] have studied different specimens of bonded and unbonded internal tendons where grout or wax is used as filling duct material. A simplified FE modelling approach using beam elements is proposed to increase computational efficiency.

Concerning external bonded tendons, Vonk et al. [6] have developed a detailed FE model to simulate a tendon de-tensioning process, considering

external elements as deviators and anchorages. Elastoplastic behaviour of strands is considered and damage is assumed in the strands and the grout, but the interaction between them is not considered.

Regarding re-anchoring, Aparicio et al. [22] have studied it in grouted monostrand tendons. A numerical model validated with experimental tests has been developed to assess the sensitivity of parameters such as the elastic modulus of the grout, the length, the mesh, and the friction coefficient in stress redistribution when there is wire breakage. The wires are modelled as Timoshenko beam elements and the grout and the sheathing duct as 3D solid elements. The contact between wires and between outer wires and grout has been considered frictional. They have observed a weak influence of the grout elastic modulus in re-anchoring. Hence, in wire re-anchoring, wire-wire friction seems to have more influence than grout-wire friction. Nevertheless, it has to be noted that this phenomenon differs from the re-anchoring of a whole strand.

To assess the bond behaviour between the strands and the grout, Wang et al. [23] have proposed a bond-slip model to represent the interface between the multi-strand tendons and the grout, taking into account the quantity, arrangement and spacing of the strands. This method derives the maximum bond, integrating it into the bond-slip relationship for a more accurate bond characterization. Guo et al. [24] have studied the bond-slip behaviour of prestressing strands of post-tensioned concrete beams, focusing on grouting defects. These defects reduce bond strength by decreasing the contact area, which subsequently reduces adhesion and friction. Grout injection defects reduce bond stresses and flatten bond–slip curves.

In contrast to the former research works, this paper focuses on the development of a FE modelling approach to reproduce the degradation process of multi-strand grouted tendons under corrosion conditions. The proposed FE modelling method is suitable for assessing the risk of failure of a tendon affected by a certain corrosion extent. This is determined by two main factors: i) the corrosion degree, which is modelled by the stress-strain law assumed by the corroded strands, and ii) the number of corroded strands of the tendon. Thus, the objective is to determine the necessary number of broken strands to achieve tendon failure. This has been studied for tendons with different initial stressing force and can be useful in bridge inspections, where the risk of tendon breakage needs to be assessed and consequently, the necessary repair actions must be determined.

The outline of this paper is as follows: In Section 2, the FE modelling approach is described as well as the experimental tests used for its validation, previously carried out by Lee and Kang [13]. Geometry, boundary conditions, and the material constitutive models are explained with particular emphasis on the constitutive model of corroded strands. In Section 3, the experimental tests of Lee and Kang [13] are numerically reproduced by the proposed modelling approach as a validation procedure. In Section 4, the parametric study is carried out, the main parameters used to define the corrosion condition of the tendon are explained, as well as the different case studies carried out, and the results obtained are discussed. Finally, Section 5 addresses some conclusions and provides future works.

2. FE modelling approach

This section presents the FE modelling approach of an external grouted post-tensioning tendon proposed in this paper. First, the experimental tests used for the validation are presented.

2.1. Experimental tests used for validation

The tendon studied by Lee and Kang [13] is a seven-strand tendon with a total length of approximately ten metres. The experiment consists of inducing accelerated and localised corrosion to the tendon strands by a galvanic corrosion cell. The corrosion process affects only five of the strands and is applied sequentially, that is, one of the strands is corroded until its breakage, then the corrosion cell is applied to another strand, and so on, until five strands are broken. To carry out the corrosion process, the grout and the duct are removed in a 30 cm region of the tendon, leaving the strands exposed. The results that are used for the modelling validation are: i) the decrease of the first four natural frequencies of the tendon with the increase of damage and ii) the decrease of the effective tensile force with the increase of damage. In their experiments, damage is defined as the quotient between the number of broken strands and the total number of strands of the tendon, as:

$$D = \frac{N_B}{N}, \tag{1}$$

where N_B is the number of strands broken in the tendon and N is the total number of strands. Thus, the same definition of damage has been used hereof.

2.2. Geometry, boundary conditions and mesh of the FE model

Two different tendons are proposed to be modelled, varying only in two geometrical properties: the number of strands and the position of the corroded section.

The first tendon, Figure 4 (a), is used to validate the modelling methodology by comparison with the aforementioned experiments; this validation is presented in Section 3. It is a seven-strand tendon with a total length of 10 m, the central 30 cm of the tendon is modelled without grout. The sheathing duct is not directly included in the model geometry; this point is discussed later in Subsection 2.3. A diameter for the tendon of 58 mm is considered, corresponding to the assumed internal diameter of the duct. The grout density considered is 2030 kg/m^3 and the sheathing duct density is 962 kg/m^3. As the duct is not included in the model, an equivalent grout density of 2286 kg/m^3 is finally adopted.

The second tendon, Figure 4 (b), is the one used for the parametric study in Section 4, it is a 19-strand tendon, which corresponds to a typical configuration used in external post-tensioning construction [25], [26]. Corrosion mainly affects at, or near the anchorage region, as this is more exposed to corrosive agents and poor grouting conditions [27]. Thus, a 40 cm region of the anchorage is modelled without grout. An internal diameter of the sheathing duct of 95 mm is assumed [28] and, again, is not included in the model geometry, although its weight is included.

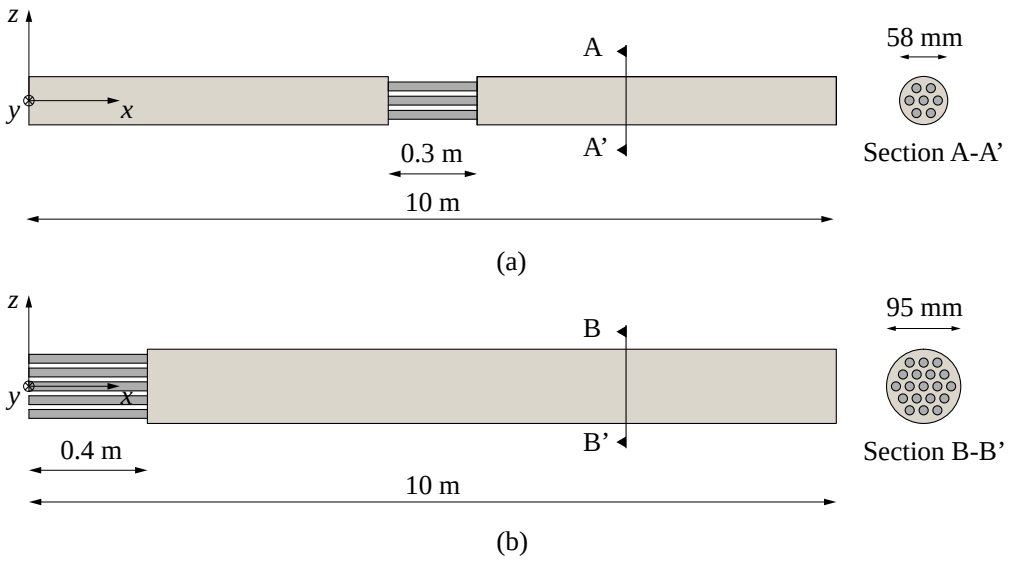

Figure 4: Geometry of the FE models used to reproduce the tendons studied. (a) Tendon 1: Benchmark case of study. (b) Tendon 2: Parametric study.

The considered strands consist of seven wires with six external wires helically surrounding a central one. Usually, an equivalent circular section is assumed, as illustrated in Figure 5, with an equivalent elastic modulus, E_s, and an effective area of a strand, A_{st}, which is 140 mm^2 [29]. Thus, the equivalent diameter, ϕ_{eq}, is:

$$A_{st} = \frac{\pi \phi_{eq}^2}{4} \rightarrow \phi_{eq} = 13.35mm, \tag{2}$$

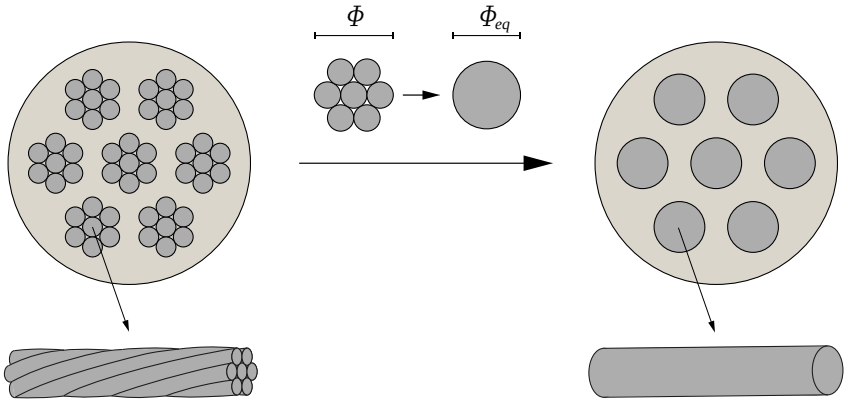

Figure 5: Illustration of equivalent strand geometry considered for FE analysis.

The boundary conditions used in this model are fixed supports at both ends of the strands. The model is developed in ANSYS Workbench and SOLID186 elements are used, so the displacements of the strand edges are constrained in all directions. SOLID186 is a high-order element that employs quadratic shape functions, allowing an accurate representation of curved geometries and non-linear deformations. It achieves higher accuracy with fewer elements and less mesh refinement than lower-order elements, supporting complex material models such as plasticity, large deformations, and non-linear stress-strain relationships. Full integration of elements is used. Meshing is developed by applying two mesh controls: i) sweep method in the strands and the grout to match their nodes, obtaining elements whose longitudinal size is 25 mm, and ii) face sizing in the strands cross-section with an element size of 5 mm and a face sizing in the grout cross-section with an element size of 15 mm. In this way, the size of the mesh elements is controlled in the longitudinal and transverse directions. Shared nodes

are considered to model the interface between the strands and the grout to achieve a conformal mesh. Moreover, a comparison between the proposed mesh and a more refined mesh has been conducted to evaluate the efficiency of the analysis. The refined mesh consists of 3 mm elements in the tendon cross-section and 10 mm elements in the longitudinal direction for both the strands and grout. The results demonstrate negligible differences between the two meshes, exhibiting similar tendon behaviour within the breakage zone and beyond the transfer length. Thus, the mesh has been chosen to achieve a trade-off between computational efficiency and result accuracy, ensuring that the analysis can be completed in a reasonable time without compromising the reliability of the results. The final mesh obtained is shown in Figure 6.

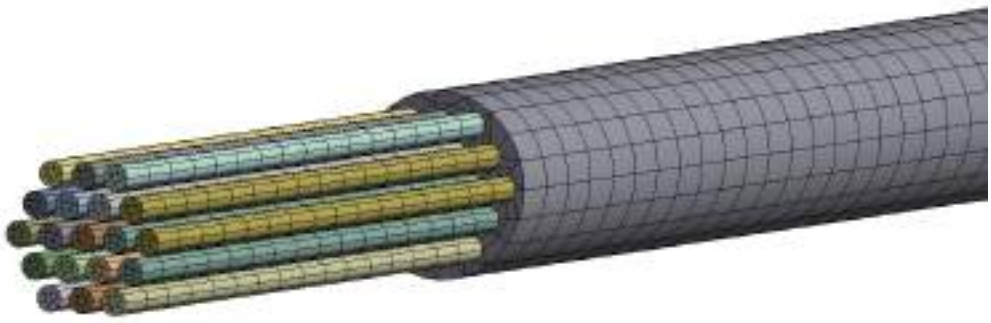

Figure 6: Example of FE mesh used for the analyses.

2.3. Material constitutive models

2.3.1. Grout: perfectly elastic to neglect the sheathing duct

Tendons have three different materials, but only two have been defined: the prestressing steel of the strands and the grout. In the analysis, the

presence of the sheathing duct has been neglected. Instead, its mechanical behaviour, explained hereafter, is modelled using a perfectly elastic grout with a higher density. When a strand breaks it tends to penetrate into the grout; however, the stiffness of the contact between the strands and the grout prevents this penetration, resulting in re-anchoring of the strand. Along the re-anchoring length, the strand recovers its initial tensile stress, while the grout undergoes longitudinal compression. This longitudinal compression causes the grout to expand radially, being this expansion effectively confined by the duct, which acts as a "belt", as shown in Figure 7. Without the duct, the grout would develop significant tensile stress in the transverse direction, leading to failure and loss of effective re-anchoring. Therefore, the influence of the duct has been considered by modelling a perfectly elastic and non-breaking grout with an elastic modulus, E_g, of 25 GPa.

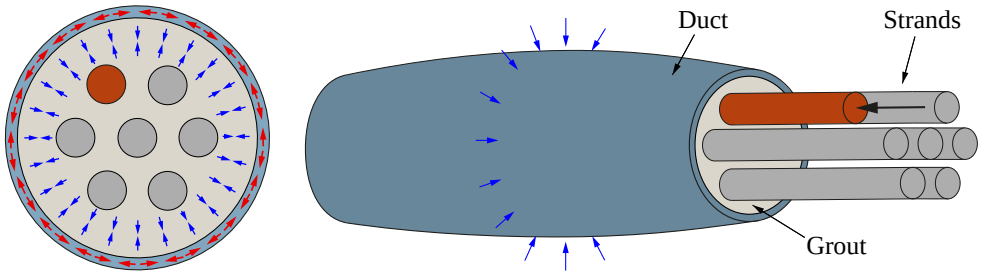

Figure 7: Effect of radial confinement of the duct on the grout when a strand breaks.

2.3.2. Uncorroded strands: bilinear isotropic hardening

A bilinear isotropic hardening material model, shown in Figure 8, has been used for the steel strands [30]. Its mechanical properties are listed in Table 2: i) the elastic modulus, E_s, ii) the yielding stress, f_{py}, iii) the yielding

strain, ε_{py}, iv) the ultimate stress, f_{pu}, v) the ultimate strain, ε_{pu}, and vi) the steel density, ρ_s. The von Mises plasticity criterion and associative plastic flow rule have been considered for the elastoplastic behaviour of the strands.

Table 2: Mechanical properties of uncorroded strand.

E_s [GPa]	f_{py} [MPa]	ε_{py} [%]	f_{pu} [MPa]	ε_{pu} [%]	ρ_s [kg/m^3]
195.5	1760	0.9	1900	6	7850

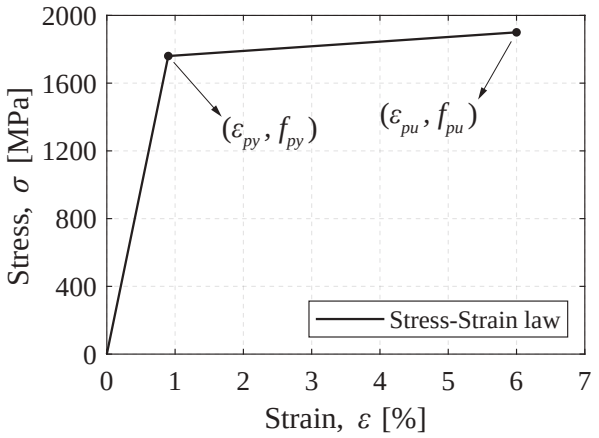

Figure 8: Uncorroded strand stress-strain law.

2.3.3. Corroded strands: steel weakening due to corrosion

Before defining a specific law to model the degradation of the mechanical properties of corroded strands, a brief review of the available literature on the topic is conducted.

Jeon et al. [31] have estimated the mechanical properties of corroded prestressing strands by tensile tests and have proposed a stress-strain law derived from a FE analysis. The properties of the corroded ultimate state

depend on the corrosion shape of the wire. An equivalent spring-based model is adopted to derive a simplified material model of a corroded strand. Zhang et al. [32] have proposed an analytical model to predict the stress-strain law of corroded strands, which has been verified with experimental tests. The constitutive model is similar to the uncorroded one, but the ultimate strain varies with the corrosion degree, as the study determines that this is the most affected parameter. Wang et al. [33] have suggested a bilinear model based on experimental tests similar to those carried out by Zhang et al. [32]. The same elastic modulus is assumed for corroded and uncorroded strands, as it shows minimum variation, and it is assumed a variation of the yield and ultimate stresses and strain when the corrosion degree increases. Franceschini et al. [34] have proposed a new constitutive trilinear law named CPS (Corroded Prestressing Strands) model, which is based on conducted tensile tests. Again, the same elastic modulus is considered as well as the decrease in the ultimate stress and strain with increasing corrosion degree.

The following relevant conclusions are drawn for the adoption of the constitutive model for corroded strands: i) there is negligible variation in the elastic modulus when a strand suffers corrosion, ii) the ultimate strain is significantly reduced with corrosion, and iii) the yield and ultimate stresses slightly decrease with corrosion. Taking into account this experimental evidence, the stress-strain law adopted for corroded steel strands is presented in the following subsection.

Stress-strain law of corroded strands

A bilinear stress-strain law is considered for corroded strands. The con-

stitutive model for corroded strands is dependent on the corrosion degree, ρ, which indicates the reduction in strand cross-section due to corrosion, as follows:

$$\rho = \frac{A_c}{A_{st}}, \tag{3}$$

where A_c is the loss of sectional area of the strand due to corrosion.

Wang et al. [33] define the critical corrosion degree, ρ_{cr}, as the minimum value for which the ultimate stress and the ultimate strain of a corroded strand do not change significantly. The value they propose for ρ_{cr} is 10.4% and is obtained based on experimental tests [33]. Zhang et al. [32] experimentally define this value of ρ_{cr} as 11%. For corrosion degrees higher than the critical value, the stress-strain law of corroded strands is assumed to be single-linear and it is coincident with the elastic branch of uncorroded strands. Thus, the stress-strain law to be used depending on the corrosion degree is the following [33]:

$$\sigma = \begin{cases} \rho \leq \rho_{cr} & \begin{cases} E_s\varepsilon & \varepsilon \leq \varepsilon_{py,c}(\rho) \\ f_{py,c}(\rho) + E_{pp}(\varepsilon - \varepsilon_{py,c}(\rho)) & \varepsilon_{py,c}(\rho) < \varepsilon \leq \varepsilon_{pu,c}(\rho) \end{cases} \\ \rho > \rho_{cr} & E_s\varepsilon \qquad \varepsilon \leq \varepsilon_{py,c}(\rho) \end{cases} \tag{4}$$

where, $f_{py,c}$ is the yield stress of the corroded strand, $\varepsilon_{py,c}$ is the yield strain of the corroded strand, $f_{pu,c}$ is the ultimate stress of the corroded strand, $\varepsilon_{pu,c}$ is the ultimate strain of the corroded strand and E_{pp} is the plastic hardening modulus of the strand. Within their contribution, Wang et al. [33] provide the necessary expressions, experimentally obtained, to compute the values of $f_{py,c}$, $\varepsilon_{py,c}$, $f_{pu,c}$, $\varepsilon_{pu,c}$ as a function of ρ.

In Figure 9 (a), it can be seen that the values of E_s and E_{pp} barely vary with ρ. Furthermore, $f_{py,c}$ does not change substantially with ρ, according to Wang et al. [33], it tends to decrease by 10% when ρ changes from 0 to 27.5%. The only parameter that significantly varies between corroded and uncorroded strands is the ultimate limit strain $\varepsilon_{pu,c}$, which registers a decrease of up to 65%. For this reason and simplicity, the stress-strain curves used for corroded strands have the same elastic branch and a shorter plastic branch up to $\varepsilon_{pu,c}$, as represented in Figure 9 (b). This is the stress-strain law for corroded strands proposed by Zhang et al. [32] and it is adopted here.

$$\sigma = \begin{cases} \rho \leq \rho_{cr} & \begin{cases} E_s\varepsilon & \varepsilon \leq \varepsilon_{py} \\ f_{py} + E_{pp}(\varepsilon - \varepsilon_{py}) & \varepsilon_{py} < \varepsilon \leq \varepsilon_{pu,c}(\rho) \end{cases} \\ \rho > \rho_{cr} & E_s\varepsilon \quad \varepsilon \leq \varepsilon_{py} \end{cases} \tag{5}$$

in which it is assumed that the ultimate strain of corroded strands follows the subsequent expression:

$$\varepsilon_{pu,c}(\rho) = \varepsilon_{pu} - \frac{\rho}{\rho_c}(\varepsilon_{pu} - \varepsilon_{py}) \tag{6}$$

As a condition, a similar constitutive law is adopted for corroded and uncorroded strands by simply changing the ultimate strain as a function of the corrosion degree. The main advantage is that it is not necessary to vary the constitutive law of some strands from a healthy state to a corroded one along the analysis, which would require a specific additional subroutine.

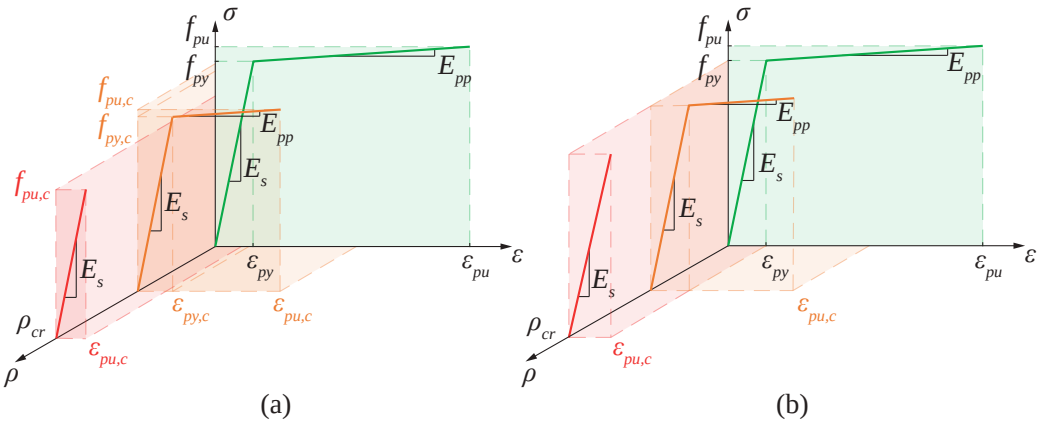

Figure 9: Stress-strain law of corroded strands: (a) based on Wang et al. [33], (b) based on Zhang et al. [32].

2.4. Type of analysis

To reproduce the degradation process of external post-tensioning tendons due to the progressive breakage of their composing strands, a non-linear static analysis divided into different load steps is performed. During the analysis, all the steps related to tendon construction (strands tensioning, tendon grouting) and tendon degradation (progressive corrosion of strands) are modelled. The non-linearity is caused by different factors: i) the non-linear constitutive law of the steel strands, ii) the large deformation analysis has to be considered, iii) the activation of grout elements to reproduce grout injection, and iv) the elimination of strands' elements when they surpass their ultimate limit stress to reproduce their breakage. A sparse direct solver and the full Newton-Raphson algorithm with convergence in forces and displacement have been used. The steps of the analysis are different depending on which tendon is being analysed i) the benchmark case of study used for the valida-

tion, Figure 4 (a) or ii) the tendon used for the parametric study, Figure 4 (b). These steps will be detailed in the following sections.

3. Model validation with experimental results

3.1. Benchmark case of study

In this section, a benchmark numerical case of study is explained to be used for model validation. The tendon tested by Lee and Kang [13], presented in Subsection 2.2 and in Figure 4 (a), is now modelled following these steps:

1. Stressing of the strands by applying a thermal load, Figure 10: Step 1. The stressing of the strands was executed at 70% of their ultimate stress, f_{pu}. A temperature decrease ΔT equal to:

$$\Delta T = \frac{0.7 f_{pu}}{E_s \alpha}, \tag{7}$$

   where α is the thermal expansion coefficient, taken as $1.2 \cdot 10^{-5}\ ^{\circ}C^{-1}$, is applied.
2. Activation of the grout to simulate injection, Figure 10: Step 2.
3. Successive breakage of five strands by eliminating elements, Figure 10: Steps 3 to 7.

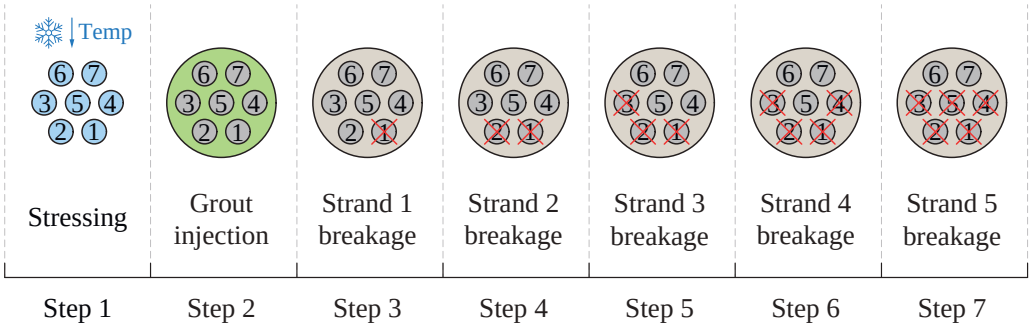

Figure 10: Steps of the analysis of the benchmark case of study used for the model validation.

The validation of the FE model is carried out by comparing the FE results with the experimental ones obtained by Lee and Kang [13]. The influence of three factors are previously studied: i) the re-anchoring length of the strands, ii) the plasticity of the strands, and iii) the large-displacement analysis considerations. Some comments on these factors are included hereafter.

Regarding the re-anchoring, a bonded contact is used for modelling the interface of steel and grout, which results in immediate re-anchoring of the strands in the grout when breakage occurs. This contact has been modelled by sharing the nodes of the grout element with those of the strand elements at their interface.

The assumption of a bonded contact is made to simplify the model. However, the validation of the numerical model against the experimental results, presented in the following Subsection 3.2, demonstrates the suitability of this assumption. The model effectively replicates the mechanical behaviour of the tendon during strand re-anchorage into the grout, which is the critical aspect of the strand-grout contact for the parametric analysis, regardless of the

precise location where re-anchorage occurs. However, a re-anchoring length is assumed, in which the strands slide into the grout before the re-anchoring occurs, this is also known as transfer length. Losanno et al. [16] compare different standards to assess transfer length and determine that transfer length values range between $11\phi_{eq}$ and $60\phi_{eq}$. The former upper bound is provided by AASHTO [35] and does not consider the influence of prestress. Finally, the transfer length used in this paper is an intermediate value, set to $22\phi_{eq}$. The additional non-grouted length is considered as half the value of the transfer length, as the re-anchoring takes place immediately due to the bonded contact, and not following a linear trend. For this reason, the total non-grouted length is 60 cm, instead of the 30 cm used in the experiment of Lee and Kang [13]. In the case where the re-anchoring effect is not present, as when using unbonded tendons, the effective tensile force of the tendon T decreases proportionally to the area of steel section lost, so a strand breakage is noticeable if this magnitude is monitored. When using grouted tendons, re-anchoring of the broken strands occurs, this implies that the tensile force initially carried by the broken strands is partially transferred to the healthy ones and the decrease of T is not proportional to the steel section lost. Both cases have been compared in the analysis performed.

Regarding the influence of plasticity, the tensile force T in the anchorage is evaluated and the results are shown in Figure 11. Two types of constitutive behaviour of prestressing steel have been considered, i) infinitely elastic with elastic modulus E_s, and ii) elasto-plastic assuming bilinear isotropic hardening plasticity model with ultimate limit strain and stress, presented in Figure 8. These two scenarios allow an understanding of the role of plasticity in the

redistribution of forces within the tendon when a strand breaks.

With regard to the consideration of large displacements, firstly, a small-displacements analysis is performed. Large transverse displacements were observed in the tendon when an eccentric strand breaks, due to the bending forces derived from the re-anchoring of this strand. Secondly, a large-displacements analysis is carried out. Both analyses are performed considering elasto-plastic steel behaviour.

3.2. Comparison with experimental results

The present subsection compares the experimental results obtained by Lee and Kang [13] with those extracted from the FE model. These results are mainly two, the evolution of the tensile force, T and the natural frequencies f_i of the tendon with its progressive damage, D previously defined in equation 1.

The evolution of T with D in the anchorage zone, thus outside the transfer length, is shown in Figure 11. The following curves are compared in this chart: i) the experimental results with a black dotted line, ii) a linear blue curve representing the case where no re-anchoring is considered, iii) a green curve where re-anchoring, elastic strands and small-displacements analysis are considered, iv) a yellow curve where re-anchoring, elasto-plastic strands and small-displacements analysis are considered, and v) a red curve where re-anchoring, elasto-plastic strands and large-displacements are considered.

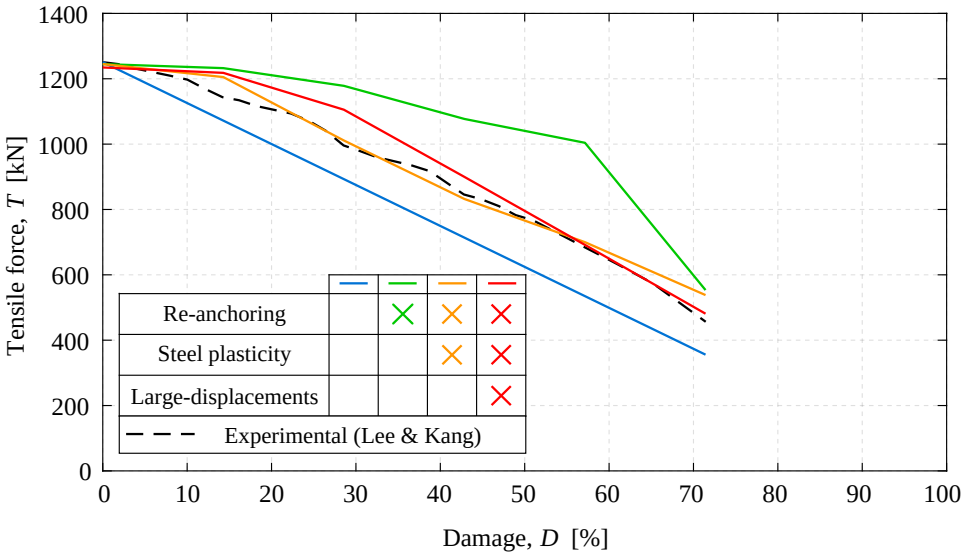

Figure 11: Degradation of the tensile force with damage in the anchorage zone.

The following conclusions are extracted from Figure 11. First, the effect of re-anchoring is clear, as when considering it, the decrease of T is non-linear to D, especially at the very first steps of the damage, where almost no force decrease is registered. Second, when re-anchoring with elastic strands is considered, as depicted by the green curve, a non-linear trend is observed; however, there are visible discrepancies with the experiments, which are clearly reduced when plasticity is considered, as illustrated in the yellow curve. Independently of considering large-displacements or not, plasticity plays a key role in the tendon's stress redistribution when a strand breaks. Third, it can be seen that when considering small-displacements with plasticity and re-anchoring, as shown in yellow curve, the results obtained in terms of T-D are similar to the experiments. Nevertheless, the evolution of T with D does

not strongly depend on the consideration of large-displacements, represented in the red curve. However, the lateral deflections observed in the case of small-displacements and the evolution of stresses around the vicinity of the breakage section within the strands are not realistic at all. This point is discussed in what follows.

The stress-strain behaviour in the vicinity of the breakage obtained at the centroid of each strand, when small-displacements and large-displacement analysis are considered, are shown in Figure 12. Figure 13 shows the same results outside the transfer length. The observed stress loss experienced by some strands in the vicinity of the breakage considering small-displacements in some strands, specifically strands 6 and 7 in Figure 12, is caused by the eccentric break of the strands inside the tendon. This implies the appearance of bending stresses in the tendon, which causes the tensioning of the strands near the broken one, and the compression of the strands located on the opposite side of the broken one. This phenomenon disappears when considering large-displacement analysis, as the effect of a broken strand is a self-stabilising action that opposes the elastic instability of the tendon. The stress-strain behaviour outside the transfer length shows the re-anchoring effect. The stresses decrease but not proportionally with the loss of steel area.

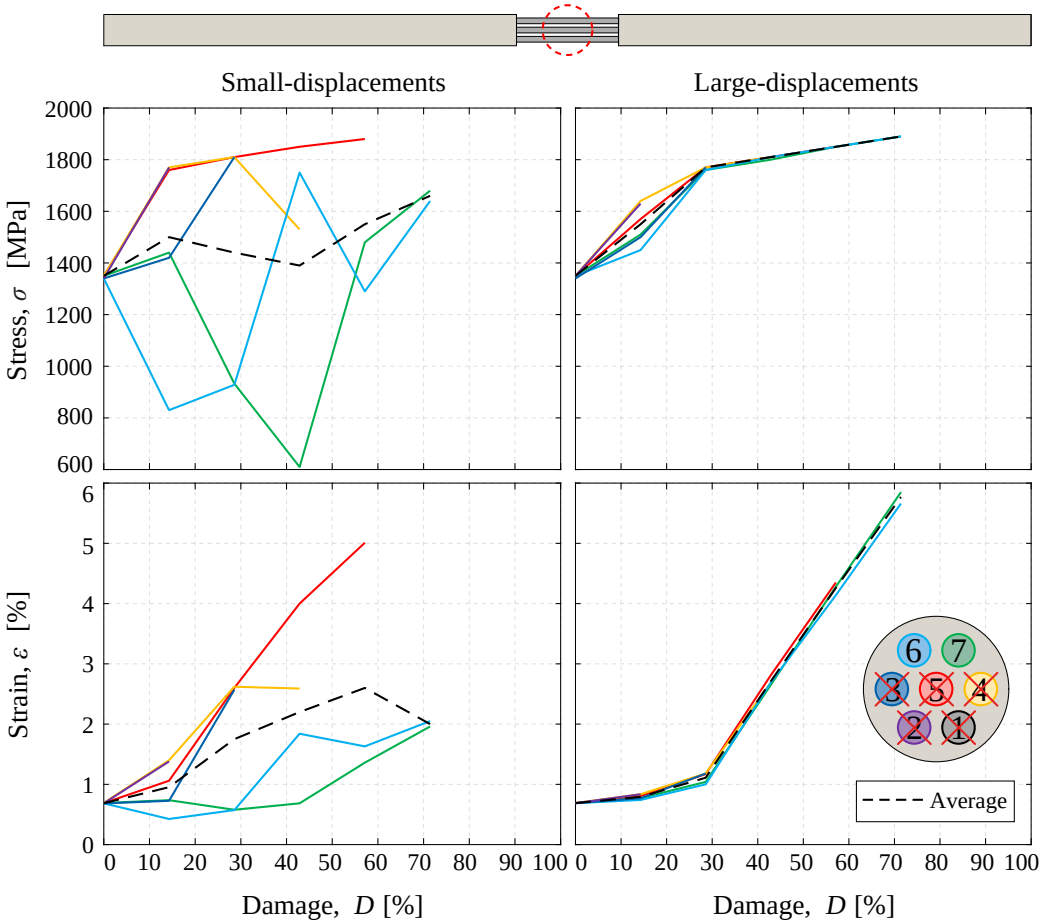

Figure 12: Stress-strain behaviour in the vicinity of the breakage considering small and large displacements.

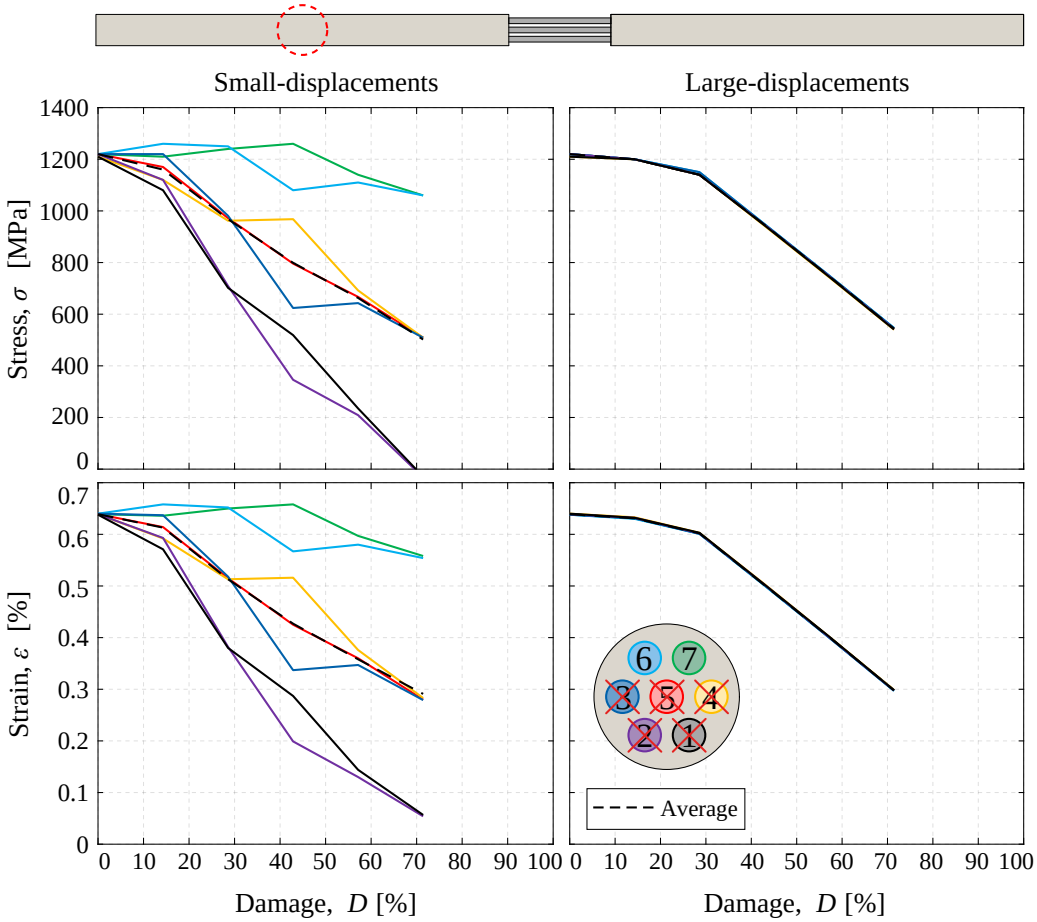

Figure 13: Stress-strain behaviour outside the transfer length considering small and large displacements.

Furthermore of Figure 12, Figure 14 shows the transverse displacements in the vicinity of the breakage considering small-displacements and large-displacements analysis. When considering small-displacements, the maximum transverse displacement reached with 70% of damage is almost 1 m, whereas, in the case of large-displacements, the maximum transverse dis-

placement reached is less than 1.4 cm. Again, this figure shows that when considering large-displacement analysis, the accuracy of the model is improved, since displacements of 1m are not realistic compared to the transversal deformation values measured by Anžlin et al. [36] and Švraka et al. [37] in damaged external grouted tendons affected by corrosion.

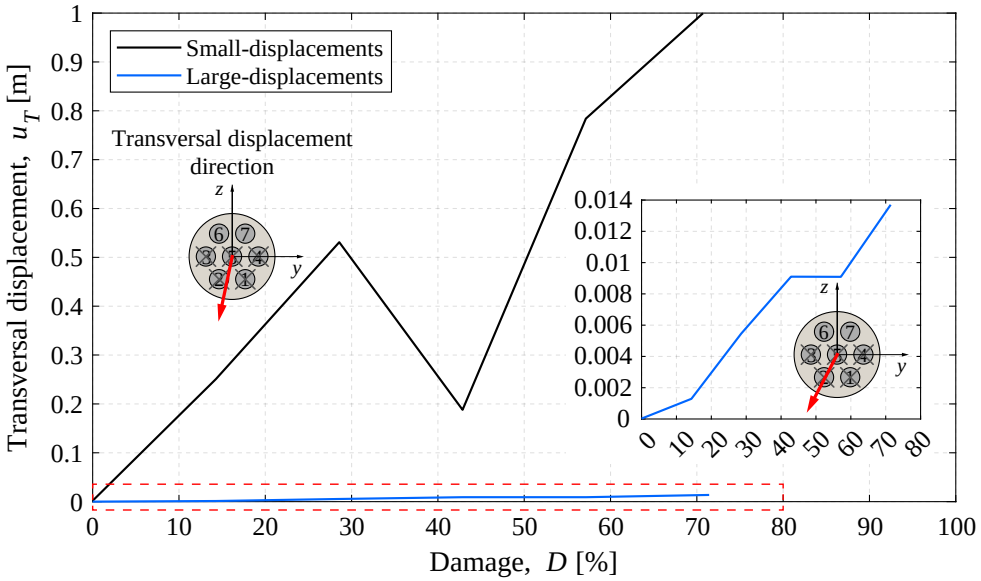

Figure 14: Transverse displacements in the vicinity of the breakage. A zoom of the results with large-displacements is included into the figure.

Finally, the evolution of the first four natural frequencies of the tendon with the damage D is also analysed using the model that considered reanchoring, plasticity of the steel strands, and large-displacement analysis. These first four frequencies are plotted together with the experimental ones in Figure 15 (a). To obtain the natural frequencies of the tendon, a linear

perturbation analysis has been performed at each step of the static analysis considering a tangent stiffness matrix of the tendon. The FE results are similar to the experimental ones, although some small discrepancies appear that might be because perfect bonding is considered in the model, and slightly higher natural frequencies are predicted by the model. Thus, the proposed modelling approach precisely reproduces the mechanical behaviour of real tendons.

Furthermore, the first ten natural frequencies are plotted with respect to the damage, D, (Figure 15). Until 30% of damage, the frequencies do not present a significant relative change, which is assumed 5%, compared to the situation without damage. The degradation in terms of the natural frequency values can be better identified by analysing the absolute values of each frequency, especially the higher ones. A key fact can be derived from the zoom shown in Figure 15 (b). For instance, the maximum absolute variation of the 10^{th} natural frequency for 10% of damage is around 2 Hz over 186 Hz, and for 30% of damage is of 9 Hz.

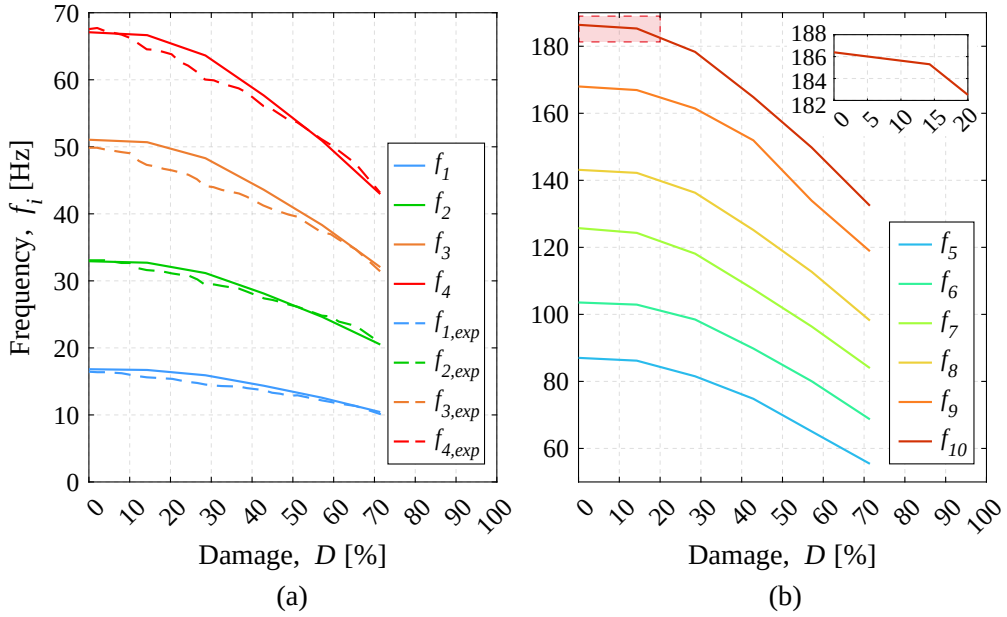

Figure 15: (a) Evolution of the first four natural frequencies with damage obtained experimentally (Lee and Kang) and numerically (proposed modelling). (b) Evolution of the 5^{th} to 10^{th} natural frequencies with damage obtained numerically.

The variation of the natural frequencies depicted in Figure 15 represents a deterministic value that excludes potential errors derived from the noise of measurement devices and the frequency estimation methodology used in in-field measurements. In long-term monitoring systems, external post-tensioning tendons are typically measured with accelerometers able to capture tendon dynamics under ambient excitations [38], [39]. Then, frequency identification procedures are commonly performed for frequency tracking and tension force estimation purposes. Consequently, tendon frequencies are expected to evolve in negative correlation with temperature changes. As a practical example, Figure 16 shows the evolution of the first seven natural

frequencies of an external grouted tendon (of similar nature to those analysed in this paper) over a month, recorded as part of a monitoring system implemented by the authors on Tremor Viaduct in Spain.

Figure 15 shows that, for instance, a 10% of damage level results in a deterministic 0.79% variation of the 7^{th} frequency. This variation would correspond to a sudden change of 0.59 Hz in the 7^{th} frequency at the tendon of Tremor Viaduct used as an example. Paying attention to the frequency time evolution of Figure 16, it is clear that the monitoring system captures perfectly well frequency variations of 0.05 Hz. Thus, analysing the time evolution of natural frequencies as structural performance indicators offers valuable insights into tendon damage, helping to detect abnormal behaviour and anticipate and prevent brittle fracture.

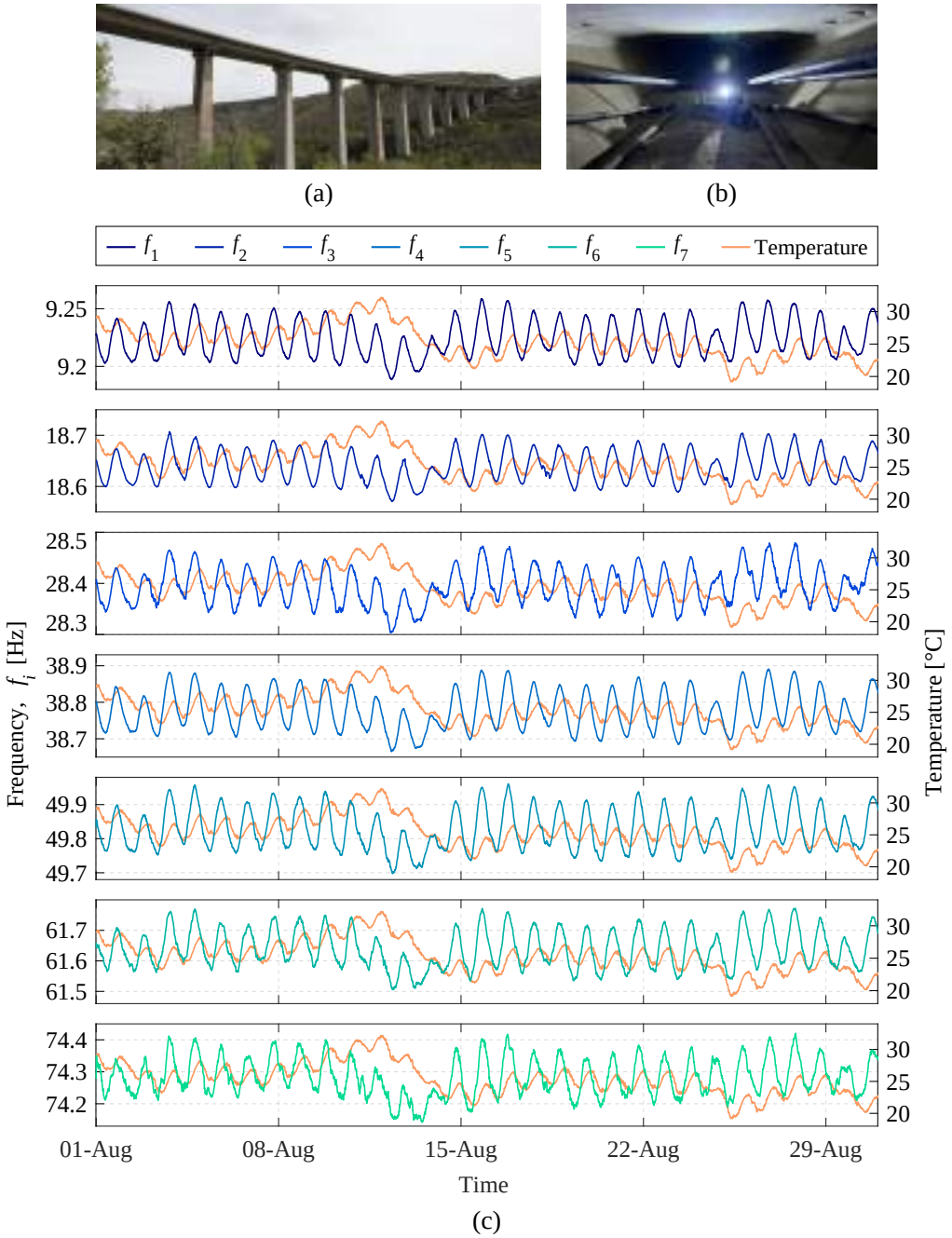

Figure 16: (a) Tremor Viaduct [40]. (b) Interior of the box girder of Tremor viaduct. (c) Temporal evolution of the first seven natural frequencies of a tendon and temperature variations at Tremor Viaduct during one month.

4. Parametric study

External grouted post-tensioning tendons present a brittle failure due to corrosion problems in the strands, mainly based on two factors: i) the re-anchoring of the broken strands into the tendon grout, and ii) the loss of ductility of corroded strands. In this context, there is significant uncertainty about the way in which the corrosion conditions of the steel strands can result in tendon failure. The modelling approach proposed enables to perform a parametric analysis to obtain the necessary number of broken strands to get the tendon failure. In this study, three main parameters have been varied:

1. Stressing force level, T_0. The initial stressing force applied determines the stress to which strands are subjected; therefore, when a strand breaks, its stresses are redistributed to the rest of the strands. On the one hand, if the stressing force level is small compared to $T_u = Af_{pu}$, the strands have a greater capacity to carry additional stresses derived from the breaking of the corroded strands. On the other hand, if the stressing force is high, approaching T_u, almost all the capacity of the strands is already depleted in the non-damage situation, so the probability of tendon failure is more sensitive to the breakage of the strands. This is illustrated in Figure 17.

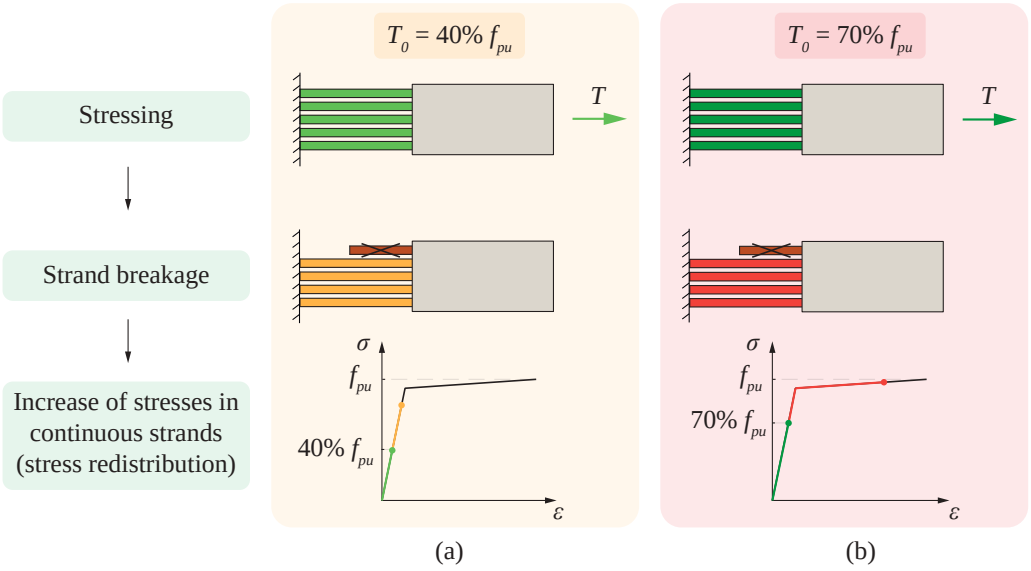

Figure 17: Stressing force influence on stress redistribution. (a) Low stressing force level. (b) High stressing force level.

2. Corrosion degree of the section, ρ. The corrosion degree is the percentage loss of the cross-section of the strands due to corrosion. As it has already been explained, the corrosion degree of the strands has been modelled by decreasing the ultimate strain $\varepsilon_{pu,c}$ of the corroded strands, considering the stress-strain law expressed in equation 5 and shown in Figure 9 (b).
3. The number of corroded strands expressed as the proportion of strands affected by corrosion, $\lambda \in [0, 1]$. This parameter is illustrated in Figure 18.

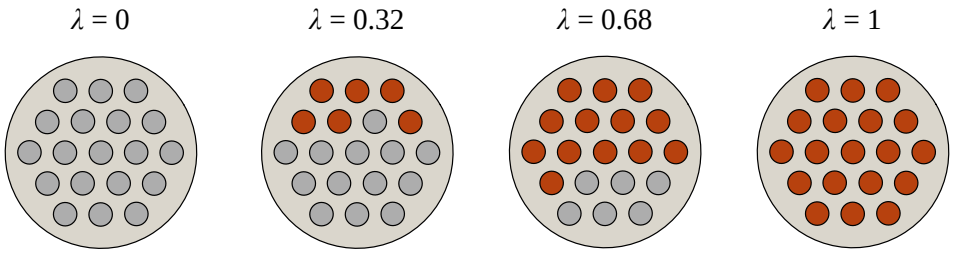

Figure 18: Proportion of the section affected by corrosion, λ.

For a given tendon with a certain number of strands and a stressing force T_0, four risk situations might be distinguished in terms of ρ and λ defining the corrosion condition of the section, as depicted in Figure 19. First, if both values are small, illustrated in dark green, the risk of failure due to a sudden strand or wire breakage is low. Second, when the corrosion degree is high but affects a small number of strands, as depicted in light green, with a low λ, the stress of the broken strand is effectively redistributed between adjacent strands, which have enough remaining ductility to assume this additional stress. Hence, the tendon resists, although some strands are broken. Critical situations arise when λ is high, as many strands of the tendon are simultaneously corroded. Two situations might happen. For high values of λ and low corrosion degree, represented by the yellow area, the risk of failure due to the strand breakage is moderate. However, for high values of λ and a significant corrosion degree, the risk of failure may become significantly high, since the corroded tendon has no more ductility margin, illustrated by the red area. In all cases, the higher the T, the higher the risk of failure.

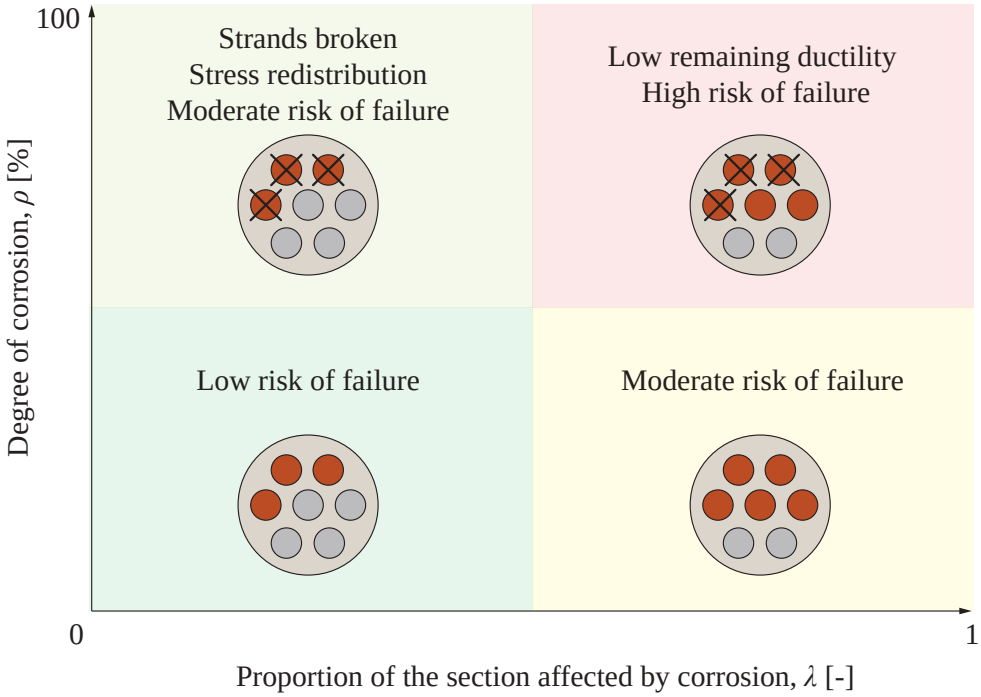

Figure 19: Corrosion status of the tendon in terms of ρ and λ.

Thus, the objective is to obtain the critical number of strands that must break to induce tendon failure, N_{crit}. An initial estimation of this number can be obtained from the capacity of non-broken strands, all of them in a healthy state, and assuming that no prestressing force loss is derived from the breakage event. This initial estimation is denoted as $N_{crit,0}$. These assumptions neglect the influences derived from the ductility of the tendons or their corrosion state. The derivation of the formula to obtain $N_{crit,0}$ is described below.

The stressing force T_0 of a given tendon with N strands, 19 in the case of the studied tendon, is usually expressed as a proportion p of its ultimate

stressing force, as follows:

$$T_0 = pNF_{pu}, \tag{8}$$

where F_{pu} is the ultimate stressing force of a strand, equal to $F_{pu} = A_{st}f_{pu}$.

The tendon will fail when $N_{crit,0}$ strands break and the same force T_0 needs to be assumed by the rest of the strands working at the ultimate stress. In this situation, the following equation is fulfilled:

$$T_0 = (N - N_{crit,0})F_{pu}, \tag{9}$$

equating equations (8) and (9), it can be concluded that $N_{crit,0}$ is equal to:

$$N_{crit,0} = N(1 - p), \tag{10}$$

dividing the above equation by N, a critical value of $\lambda_{crit,0}$ is obtained:

$$\lambda_{crit,0} = (1 - p). \tag{11}$$

This value indicates that when the proportion of the steel section strongly corroded is higher than $\lambda_{crit,0}$, the risk of failure suddenly increases. Furthermore, this expression confirms that the risk of failure is inversely proportional to the stressing level of the tendon, p.

4.1. Studied cases

The parametric analysis performed is focused on determining λ_{crit}, the critical proportion of strands that should break at the same time to cause global failure of a tendon, from the proposed modelling approach. This finer estimation also considers the influence of the ductility of the healthy strands

and the tendon's corrosion conditions. The study considers five different stressing forces, with the following stressing levels: $p = 0.4$, $p = 0.5$, $p = 0.6$, $p = 0.7$ and $p = 0.8$ (Equation 8). For each of them, two corrosion degrees are studied: $\rho_1 = 11\%$, which corresponds to ρ_{cr}, and $\rho_2 = 5.5\%$. The corrosion degree ρ_1 is the one in which the corroded ultimate strain, $\varepsilon_{pu,c1}$ is equal to the uncorroded yield strain, ε_{py}, as illustrated in Figure 20 (a). Whereas the corrosion degree ρ_2 is the one corresponding to a corroded ultimate strain, $\varepsilon_{pu,c2}$, that is half of the plastic branch of the uncorroded stress-strain law, as shown in Figure 20 (b), that is:

$$\varepsilon_{pu,c2} = \varepsilon_{py} + \frac{\varepsilon_{pu} - \varepsilon_{py}}{2} \tag{12}$$

.

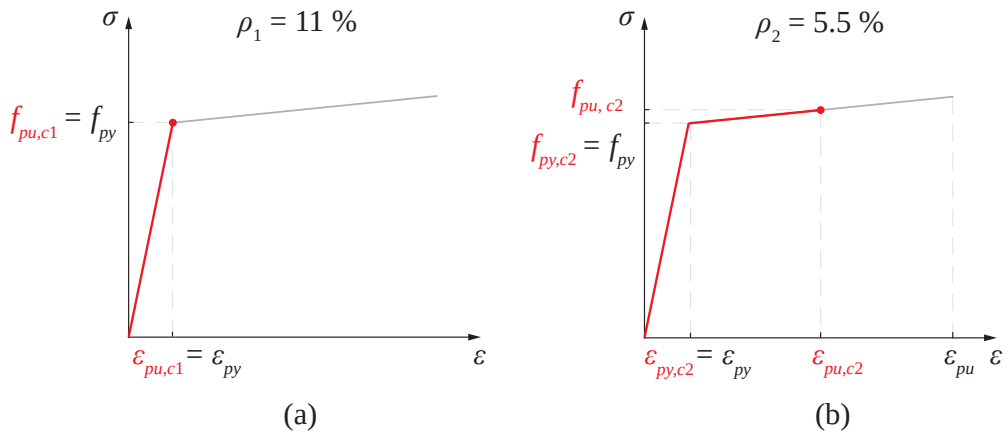

Figure 20: Stress-strain constitutive law for both corrosion degrees considered.

Furthermore, each case of study resulting from a combination of p and ρ has been assessed by varying the corroded area λ from 0% to 100% each 10%. For each case, the proportion of strands that need to break to cause

tendon failure, λ_{crit}, has been obtained. Thus, the studied cases include the following values of these parameters:

1. $\rho \in [5.5, 11]\%$.
2. $\lambda \in [0 : 10 : 100]\%$.
3. $p \in [40, 50, 60, 70, 80]\%$

In each of the cases studied, these are the analysis steps that are followed, shown in Figure 21:

1. Stressing of strands by applying a thermal load.
2. Activation of the grout to simulate injection.
3. Corrosion. This is modelled by activating the ultimate stress-strain state of the corroded strands.
4. Breakage of a corroded strand.
5. Stress verification of the rest of the strands and elimination of elements above the ultimate limit strain. There are different values in the case of a corroded or an uncorroded strand.
6. Verify if the tendon failure has occurred. If all strands are broken due to the elimination of elements above the ultimate limit strain, tendon failure is reached, and the analysis finishes. If not, the number of strands initially broken in Step 4 is increased until the failure is achieved. When the tendon fails, the critical number of strands N_{crit} that have produced the collapse is obtained for each case.

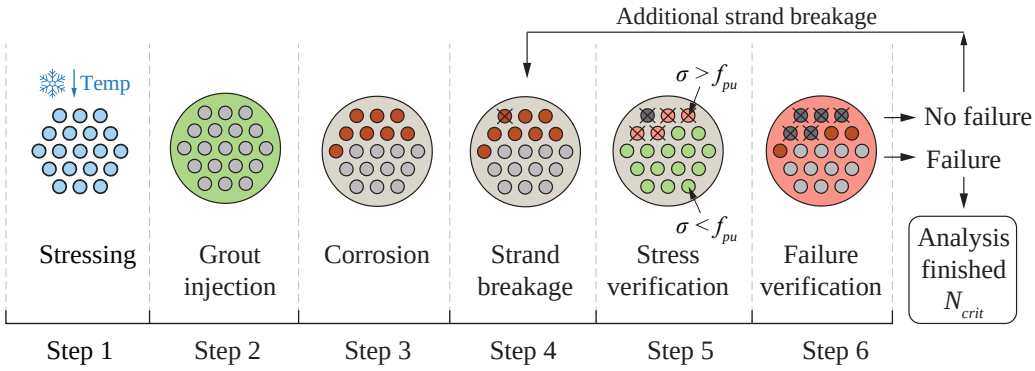

Figure 21: Steps of the analysis of the tendon used for the parametric study.

4.2. Results of parametric study

The results of the analysis are presented in Figure 22. Figure 22 (a) refers to the tendons with a corrosion degree of ρ= 11%, and Figure 22 (b) refers to those with a corrosion degree of ρ= 5.5%. Each of the curves included represents one study case in which the different stressing levels studied are considered.

With no corroded area, $\lambda = 0\%$, the proportion of broken strands that a tendon can assume without reaching its failure depends on the stressing force. For the stressing forces considered in this study, this value is obtained. If the tendon is stressed at $0.8f_{pu}$ in the case of a 19-strand tendon, 7 strands should break to produce the tendon failure, which represents 37% of the steel section (λ_{crit}). This is considerably higher than $\lambda_{crit,0}$ = (1-0.8)100 = 20%. Respectively, for a lower stressing force as $0.6f_{pu}$, the proportion of steel section that should break for tendon failure increases to 63%, as well as the difference with $\lambda_{crit,0}$, which increases to 40%. Furthermore, when the tendon is stressed at $0.4f_{pu}$, the difference between λ_{crit} and $\lambda_{crit,0}$ becomes even

more pronounced, suggesting that this difference increases as the stressing force level decreases.

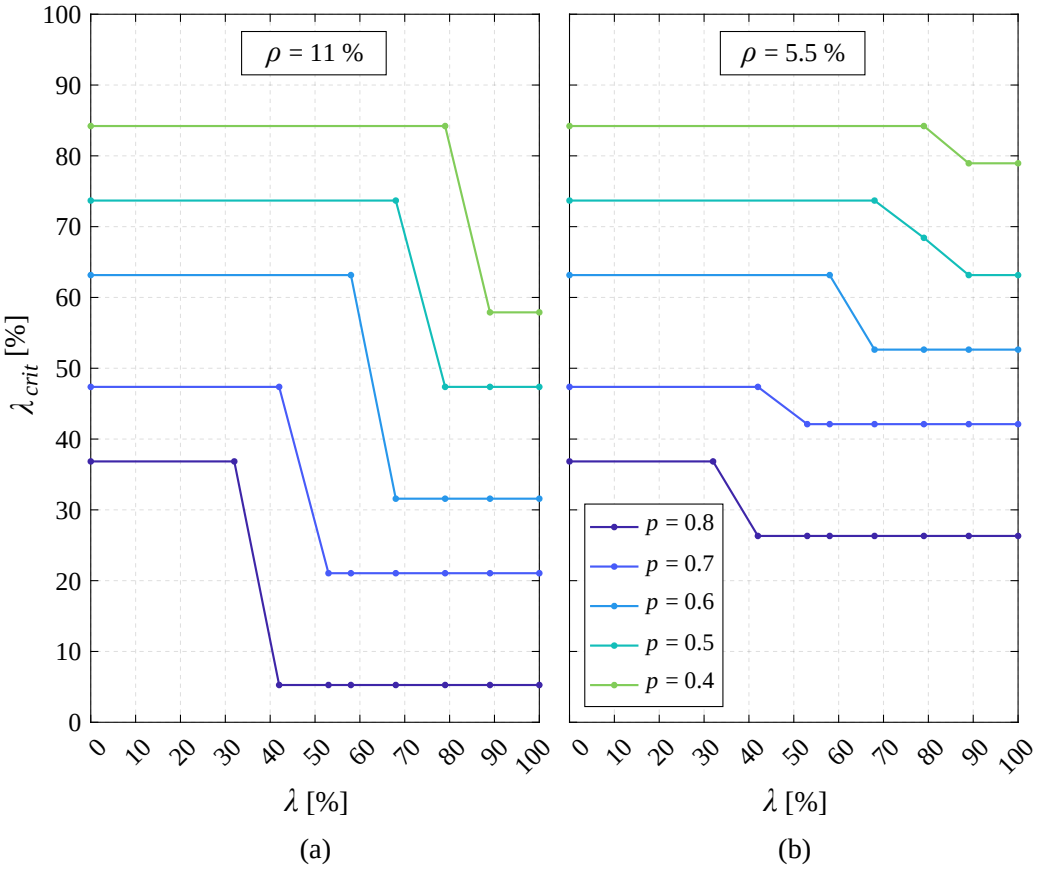

Figure 22: Proportion of broken strands resulting in tendon failure for a given p and ρ in terms of λ. (a) $\rho = 11\%$. (b) $\rho = 5.5\%$

The results obtained show the high influence of the stressing force on the risk of tendon failure. In the case of a tendon stressed at $80\% f_{pu}$ with a corrosion degree equal to 11%, Figure 22 (a), when λ is lower than 32%, λ_{crit} is kept as a constant value equal to 37%, which corresponds to 7 strands. This

is because in this case all the corroded strands are broken and, after that, the remaining steel area is healthy. However, when λ increases from 32% to 42%, the critical number of broken strands suddenly decreases to 1, or $\lambda_{crit} = 5\%$. This means that above this value, the redistribution capacity of the tendon is small and there is a clear lack of ductility. In these situations, a knock-on effect occurs when 1 strand breaks, causing the tendon to collapse. This is the most risky case, since it has the highest stressing force and the highest corrosion degree, so the strands have a small capacity for stress redistribution. When the corrosion degree is 5.5%, as shown in Figure 22 (b), the available ductility in the corroded strands causes the disappearance of the sudden decrease seen in the case of a higher corrosion degree. In this case, it is ensured that at least 26% of the section, which corresponds to 5 strands, must break to cause tendon failure, regardless of the corroded area.

If the tendon is stressed at a lower level, the results provide greater structural safety about tendon failure for both of the corrosion degrees studied. In the case of a tendon stressed at $40\%f_{pu}$, for the 11% corrosion degree, the tendon fails when 16 strands break ($\lambda_{crit} = 84\%$) if the proportion of corroded strands is below 80%, if this value increases, suddenly decreases to 11 (58%). For the 5.5% corrosion degree, the most favourable case is given. It takes 15 broken strands (79%) and a proportion of corroded strands greater than 89% to cause tendon failure. Therefore, for a small corrosion degree and a lower stressing force, it is unlikely that the tendon will fail.

The loss of ductility in the strands becomes critical when there is a pronounced decrease of λ_{crit}. The point where this decrease is produced is independent of the corrosion degree but is influenced by the stressing force

level. Predicting the situation in which this decrease occurs is crucial, as inspections could prevent reaching this critical point, which is independent of the corrosion degree. In Figure 23 (a) this trend has been obtained for the 19-strand tendon studied. However, the magnitude of this decrease, called $\Delta\lambda_{crit}$, is highly dependent on the corrosion degree and is not affected by the stressing force level. The average $\Delta\lambda_{crit}$ as a function of ρ is shown in Figure 23 (b). In this way, knowing the corrosion degree, $\Delta\lambda_{crit}$ can be estimated, allowing a rapid prediction of λ_{crit} for tendons with a significant number of strands impacted by corrosion.

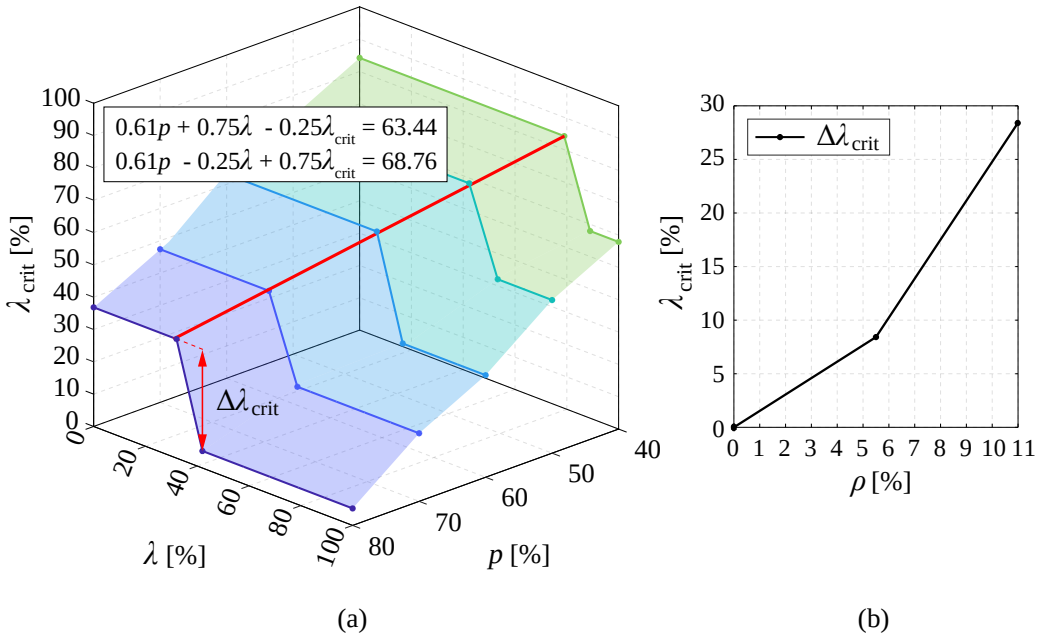

Figure 23: (a) Evolution of the critical threshold for ductility loss. (b) Evolution of $\Delta\lambda_{crit}$ in terms of ρ.

The obtained results in the parametric study highlight the influence of the

parameters analysed. The presence of a 5.5% or an 11% corrosion degree for the same stressing force results in a 21% difference in the number of broken strands required for tendon failure, for both stressing levels. The influence of stressing force is notable, starting with the proportion of broken strands that the tendon resists without corrosion $\lambda_{crit,0}$, there is a 47% difference in the steel section that can be lost before the tendon failure between the highest and lowest stressing levels studied. After this analysis, it can be concluded that when assessing the risk of failure of a given grouted post-tensioning tendon, the following questions must be made related to the studied parameters from most to least important: i) what is the initial stressing level of the tendon? If the answer is high, ii) what is the corrosion degree of the strands? If the answer is high, iii) what is the proportion of corroded strands in the worst section?

To apply this parametric study as a practical tool in bridge inspections, engineers must estimate and quantify the three input parameters used in the modelling approach. The use of non-destructive testing (NDT) techniques can assist the engineer in this task. Before quantifying these parameters, it is essential to detect potential corroded zones by evaluating all anchorages and identifying visible defects in the sheathing duct, such as cracked, swollen or visibly deviated tendon sections [37], [11]. Then, the following NDT techniques are recommended for the estimation of each parameter:

1. The tensile force T can be estimated by employing vibration response methods, taking advantage of its relationship with the natural frequencies of the tendon [41], [42]. Other alternatives include optical fiber sensors embedded in strands [43], computer vision-based technologies

[44] or X-ray diffraction measurements [45]. If the tensile force of a tendon is significantly lower than that of other similar tendons in the inspected bridge, the tendon may require re-tensioning or replacement.

2. The proportion of corroded strands λ can be determined by detecting voids in the grout that leave the strands exposed. NDT methods, such as visual inspection using borescopes, can be used for void detection [41], [42]. However, this approach is constrained to regions accessible for borescope cable insertion. Techniques as ground penetrating radar (GPR) [42] or radiography [37], [41] are suitable to detect corrosion in areas that are not easily reachable. Guided wave ultrasonic testing is particularly advantageous for tendons, as it enables long-distance monitoring and is well-suited to the tendon geometry, making it particularly effective for post-tensioning system inspections [42].
3. The corrosion degree ρ can be determined through visual inspection at anchorages by evaluating the area of steel lost, or by using the magnetic flux leakage (MFL) method. This NDT technique enables the detection and quantification of steel section loss in external post-tensioning tendons [37], providing a reliable means for evaluating the corrosion degree, as well as the proportion of corroded strands [46].

5. Conclusions

In this paper, a factly simple FE modelling approach has been presented to analyse the degradation process of external grouted post-tensioning tendons due to corrosion and estimate the residual tensile force as strands break. First, a numerical model that reproduces the 7-strand tendon tested by Lee

and Kang [13] has been carried in order to validate the proposed modelling approach. Then, this modelling approach has been used to perform a parametric study to assess the risk of failure of a tendon, evaluating the critical number of strands broken for tendon failure depending on its corrosion conditions. Thus, the following conclusions are drawn:

1. The numerical and experimental results of the degradation of the tensile force and the natural frequencies with damage are in good agreement, proving the validity of the modelling approach. The re-anchoring of the broken strands in the grout, the stress redistribution between the adjacent strands in the vicinity of the breakage, and the influence of second-order effects are taken into account by the modelling approach. This re-anchoring is crucial to explain why the tensile force does not decrease proportionally with the area of steel lost in grouted tendons.
2. The consideration of the plasticity of the strands allows to explain the decrease of the tensile force with the degradation of the tendon. Additionally, second-order geometry effects have proven to have a non-negligible influence on the deflection of the tendon caused by the breakage of eccentric strands and on the stresses present in the adjacent strands around the vicinity of the breakage section.
3. Natural frequencies show a decrease as the damage increases; this degradation is higher for higher levels of damage and for higher frequencies in absolute terms. Quantifying the absolute reduction of frequencies is important in establishing their use as an indicator of structural performance.
4. The parametric study performed based on the modelling strategy pre-

sented is a convenient tool that can be used in bridge inspections to determine the risk of tendon failure. Knowing the stressing force of the tendon and its corrosion conditions through the application of NDT techniques, it is possible to predict the number of strands that would have to break to cause its failure by using the modelling approach presented. The parametric analysis also allows to determine critical thresholds for ductility loss independently of the corrosion degree.

5. The parameters influencing the risk of tendon failure from the highest to the lowest are: i) the stressing force of the tendon T_0, ii) the corrosion degree ρ, and iii) the proportion of corroded strands λ. It is remarkable to observe that for a tendon stressed at $80\% f_{pu}$ with 42% corroded strands, the tendon collapses when only one strand breaks. These corrosion conditions might occur, for example, at the anchorage of a tilted tendon segment where the grouting might be deficient.

Future works might be focused on the direct inclusion of the duct model and on the consideration of a non-linear modelling of the grout mechanical behaviour. Furthermore, the proposed modelling approach can be used for risk assessment, and the present study may be extended to a global analysis of the response of bridge girders with corroded external postensioning. This will enable assessing the impact of the prestressing corrosion level into the bending capacity of these bridges.

6. Acknowledgements

Research project PID2021-127627OB-I00 funded by MCIN AEI/10.13039 / 501100011033/FEDER, EU. Belén Vecino acknowledges the Fundación

Agustín de Betancourt for the financial support provided for the development of her doctoral thesis.

References

[1] D. Trejo, M. D. B. Hueste, P. Gardoni, R. G. Pillai, K. Reinschmidt, S. B. Im, S. Kataria, S. Hurlebaus, M. Gamble, T. T. Ngo, Effect of voids in grouted, post-tensioned concrete bridge construction: volume 1-electrochemical testing and reliability assessment, Technical Report, Texas Transportation Institute, 2009.

[2] M. Chandoga, H.-R. Ganz, C. Kuilboer, L. Krauser, J. Piekarski, G. Ramírez, A. Windisch, External Tendons for Bridges, fib, The International Federation for Structural Concrete, 2020. doi:10.35789/fib.BULL.0097.

[3] B. Godart, Status of durability of post-tensioned tendons in France, Proceedings of a Workshop Held at Ghent University (2001) 25–42.

[4] S. Kamalakannan, R. Thirunavukkarasu, R. G. Pillai, M. Santhanam, Factors affecting the performance characteristics of cementitious grouts for post-tensioning applications, Construction and Building Materials 180 (2018) 681–691. doi:10.1016/j.conbuildmat.2018.05.236.

[5] IDEAM, Memoria Técnica de los trabajos realizados en el marco de la emergencia y estado de avance de las conclusiones de los mismos, Technical Report, MITMA. Demarcación de Carreteras del Estado en Galicia, 2022. URL: https://cdn.mitma.gob.es/portal-web-drupa

l/doc_mitma/2126c-016.0_informe_preliminar_causas_firmado.pdf.

[6] E. Vonk, A. Schwarz, A. Bonetto, Latest developments in replacing external post-tensioning tendons, Proceedings of the 11th International Conference on Bridge Maintenance, Safety and Management, IABMAS 2022 (2023) 2479–2486. doi:10.1201/9781003322641-309.

[7] S. L. Wood, C. A. McKinstry, J. K. Lee, Residual tensile capacity of grouted post-tensioned tendons, ACI Structural Journal 110 (2013) 2561–2572. doi:10.14359/51686164.

[8] J. Aparicio, T. Hoang, G. Cumunel, G. Forêt, Y. Jeanjean, J. C. Saint Martin, Mechanical impact of wires break in grouted external prestressing tendon, Academic Journal of Civil Engineering (2023). doi:10.26168/ajce.41.1.33.

[9] R. W. Poston, J. S. West, North american strategies for improving bonded post-tensioned concrete construction, Proceedings of a Workshop Held at Ghent University (2001) 245–255.

[10] M. Carsana, L. Bertolini, Characterization of segregated grout promoting corrosion of posttensioning tendons, Journal of Materials in Civil Engineering 28 (2016). doi:10.1061/(asce)mt.1943-5533.0001451.

[11] T. Kretz, J.-M. Lacombe, B. Godart, Note de sensibilisation sur les ouvrages existants à précontrainte extérieure protégée par du coulis de ciment au contact des armatures, Sétra, 2007.

[12] A. B. M. Abdullah, J. A. Rice, H. R. Hamilton, G. R. Consolazio, Experimental and numerical evaluation of unbonded posttensioning tendons subjected to wire breaks, Journal of Bridge Engineering 21 (2016) 04016066. doi:10.1061/(asce)be.1943-5592.0000940.

[13] J. K. Lee, J. W. Kang, Experimental evaluation of vibration response of external post-tensioned tendons with corrosion, KSCE Journal of Civil Engineering 23 (2019) 2561–2572. doi:10.1007/s12205-019-0735-5.

[14] D. Kim, C. H. Jeon, C. S. Shim, An experimental study on the deterioration behaviour of external tendons due to corrosion, KSCE Journal of Civil Engineering 27 (2023) 5319–5328. doi:10.1007/s12205-023-0316-5.

[15] D. Losanno, S. Galano, F. Parisi, M. R. Pecce, E. Cosenza, Experimental investigation on nonlinear flexural behavior of post-tensioned concrete bridge girders with different grouting conditions and prestress levels, Journal of Bridge Engineering 29 (2024). doi:10.1061/jbenf2.beeng-6466.

[16] D. Losanno, S. Galano, F. Parisi, Influence of strand rupture on flexural behavior of reduced-scale prestressed concrete bridge girders with different prestressing levels, Engineering Structures 301 (2024). doi:10.1016/j.engstruct.2023.117358.

[17] S. R. Ghoreishi, T. Messager, P. Cartraud, P. Davies, Validity and limitations of linear analytical models for steel wire strands under axial

loading, using a 3D FE model, International Journal of Mechanical Sciences 49 (2007) 1251–1261. doi:10.1016/j.ijmecsci.2007.03.014.

[18] F. Foti, A. de Luca di Roseto, Analytical and finite element modelling of the elastic–plastic behaviour of metallic strands under axial–torsional loads, International Journal of Mechanical Sciences 115-116 (2016) 202–214. doi:10.1016/j.ijmecsci.2016.06.016.

[19] E. A. de Menezes, T. V. Lisbôa, R. J. Marczak, A novel finite element for nonlinear static and dynamic analyses of helical cables, Engineering Structures 293 (2023). doi:10.1016/j.engstruct.2023.116622.

[20] A. B. Abdullah, J. A. Rice, H. R. Hamilton, G. R. Consolazio, An investigation on stressing and breakage response of a prestressing strand using an efficient finite element model, Engineering Structures 123 (2016) 213–224. doi:10.1016/j.engstruct.2016.05.030.

[21] N. R. Brenkus, J. Tatar, H. R. Hamilton, G. R. Consolazio, Simplified finite element modeling of post-tensioned concrete members with mixed bonded and unbonded tendons, Engineering Structures 179 (2019) 387–397. doi:10.1016/j.engstruct.2018.10.051.

[22] J. Aparicio, T. Hoang, G. Cumunel, G. Forêt, Y. Jeanjean, J. C. Saint Martin, Experimental and numerical study on the re-anchoring of wire in grouted prestressed tendons, in: Istanbul IABSE Symposium (ISTBR 2023) LONG SPAN BRIDGES, 2023.

[23] L. Wang, P. Yuan, X. Zhang, Y. Dong, Y. Ma, J. Zhang, Bond behavior between multi-strand tendons and surrounding grout: Interface equiva-

lent modeling method, Construction and Building Materials 226 (2019) 61–71. doi:10.1016/j.conbuildmat.2019.07.242.

[24] R. Guo, Z. Zhen, S. Zhao, C. Li, Effects of grouting defects in a duct on the bonding of prestressing strands, KSCE Journal of Civil Engineering 24 (2020) 1268–1275. doi:10.1007/s12205-020-0892-6.

[25] E. El Zghayar, K. R. Mackie, Z. B. Haber, W. Potter, Secondary anchorage in post-tensioned bridge systems, ACI Structural Journal 110 (2013) 629–638.

[26] W. H. Hartt, T. S. Theryo, Corrosion-Induced Failure of Bridge Post-Tensioning Tendons, CRC Press, 2020.

[27] A. Sagüés, S. Kranc, T. Eason, Vibrational tension measurement of external tendons in segmental posttensioned bridges, Journal of Bridge Engineering 11 (2006) 582–589. doi:10.1061/(ASCE)1084-0702(2006)11:5(582).

[28] Freyssinet, El pretensado de Freyssinet, 2014. URL: https://www.freyssinet.com.

[29] DYWIDAG, Sistemas DYWIDAG de postesado de cable adherente, 2008. URL: www.dywidag-sistemas.com.

[30] Model Code 2010: first complete draft, volume 1, Federation internationale du beton, 2010. doi:10.35789/fib.BULL.0055.

[31] C. H. Jeon, J. B. Lee, S. Lon, C. S. Shim, Equivalent material model

of corroded prestressing steel strand, Journal of Materials Research and Technology 8 (2019) 2450–2460. doi:10.1016/j.jmrt.2019.02.010.

[32] X. Zhang, L. Wang, J. Zhang, Y. Liu, Corrosion-induced flexural behavior degradation of locally ungrouted post-tensioned concrete beams, Construction and Building Materials 134 (2017) 7–17. doi:10.1016/j.conbuildmat.2016.12.140.

[33] L. Wang, T. Li, L. Dai, W. Chen, K. Huang, Corrosion morphology and mechanical behavior of corroded prestressing strands, Journal of Advanced Concrete Technology 18 (2020) 545–557. doi:10.3151/jact.18.545.

[34] L. Franceschini, F. Vecchi, F. Tondolo, B. Belletti, J. S. Montero, Mechanical behaviour of corroded strands under chloride attack: A new constitutive law, Construction and Building Materials 316 (2022). doi:10.1016/j.conbuildmat.2021.125872.

[35] AASHTO, LRFD bridge design specifications, 17th ed., American Association of State Highway and Transportation Officials, Washington, D.C., USA, 2014.

[36] A. Anžlin, R. Švraka, D. Hekič, U. Bohinc, Condition monitoring of external prestressing tendons on a concrete multi-span highway viaduct, in: Proceedings of the 1st Conference of the European Association on Quality Control of Bridges and Structures. EUROSTRUCT 2021, volume 200, Springer International Publishing, 2022, pp. 642–650. doi:10.1007/978-3-030-91877-4_73.

[37] R. Švraka, L. Bevc, R. Vezočnik, D. Hekič, A. Anžlin, Investigation of the unusual deformations of external tendons in concrete highway bridges, ce/papers 6 (2023) 111–117. doi:10.1002/cepa.2194.

[38] A. Cigada, F. Lucà, M. Malavisi, G. Mancini, A damage detection strategy on bridge external tendons through long-time monitoring, in: Conference Proceedings of the Society for Experimental Mechanics Series, Springer, 2021, pp. 159–168. doi:10.1007/978-3-030-47634-2_18.

[39] L. Chillitupa-Palomino, C. Barrera-Vargas, J. H. García-Palacios, I. M. Díaz, J. Naranjo-Pérez, Machine learning-based clustering and regression for assessing temperature-induced variations on external tendon's natural frequencies, in: Proceedings of the 12th International Conference on Bridge Maintenance, Safety and Management, IABMAS 2024, CRC Press/Balkema, 2024, pp. 2311–2318. doi:10.1201/9781003483755-274.

[40] Diario de León, Fomento evitará el colapso del viaducto Tremor con un refuerzo de cableado, 2023. URL: https://www.diariodeleon.es/bierzo/231025/932838/fomento-evitara-colapso-viaducto-tremor-refuerzo-cableado.html.

[41] A. B. Mehrabi, A. M. Asce, In-service evaluation of cable-stayed bridges, overview of available methods, and findings, Journal of Bridge Engineering (2006). doi:10.1061/ASCE1084-0702200611:6716.

[42] M. Taeby, A. B. Mehrabi, Risk-based selection of inspection method for

external post-tensioning system of bridges, Applied Sciences (Switzerland) 12 (2022). doi:10.3390/app12147103.

[43] C. Williams, M. Khatri, P. Okumus, R. Holt, Post-tensioning Force Measurement Using Optical Fiber Sensor-Embedded Strand for Prestressed Concrete Structures, Springer Nature Switzerland, 2023, pp. 622–633. doi:10.1007/978-3-031-32511-3_65.

[44] D. Jana, S. Nagarajaiah, Computer vision-based real-time cable tension estimation in dubrovnik cable-stayed bridge using moving handheld video camera, Structural Control and Health Monitoring 28 (2021). doi:10.1002/stc.2713.

[45] F. Morelli, I. Panzera, A. Piscini, W. Salvatore, F. Chichi, G. P. Marconi, D. Maestrini, M. Gammino, M. Mori, X-ray measure of tensile force in post-tensioned steel cables, Construction and Building Materials 305 (2021). doi:10.1016/j.conbuildmat.2021.124743.

[46] S. Salamone, I. Bartoli, R. Phillips, C. Nucera, F. L. D. Scalea, Health monitoring of prestressing tendons in posttensioned concrete bridges, Transportation Research Record (2011) 21–27. doi:10.3141/2220-03.